Intermolecular-Directed Reactivity in Solid Media. Radiogenic Formation of Phosphorus-Centered Radicals in Chiral Diphosphine Disulfides Studied by ESR

Olav M. Aagaard,*,† René A. J. Janssen,† Bas F. M. de Waal,† Jan A. Kanters,‡ Arie Schouten,‡ and Henk M. Buck†

Contribution from the Laboratory of Organic Chemistry, Eindhoven University of Technology, P.O. Box 513, 5600 MB Eindhoven, The Netherlands, and Laboratory of Crystal and Structural Chemistry, State University of Utrecht, Utrecht, The Netherlands. *Received December 8, 1989*

Abstract: Single-crystal, powder, and frozen-matrix ESR experiments have been performed to study the radiogenic electron-capture properties of several diastereoisomeric and asymmetric diphosphine disulfides ($R_1R_2P(S)P(S)R_3R_4$). The principal values of the hyperfine couplings of several phosphorus-centered radical configurations are determined and related to the spin density distribution. Attention is focused on the strong differences in radiogenic properties, observed between the meso and racemic forms of phenyl- and tolyl-substituted diphosphine disulfides. The most striking result is that X irradiation of the crystalline meso compounds MePhP(S)P(S)MePh, Me(*p*-Tol)P(S)P(S)Me(*p*-Tol), and $Ph(PhCH_2)P(S)P(S)Ph(CH_2Ph)$ does not lead to the formation of a three-electron bond P∴P σ^* radical but invariably results in configurations in which the unpaired electron is primarily localized on one half of the molecule. X irradiation of the corresponding racemic forms, on the other hand, gives rise to P∴P σ^* configurations. The observed discrimination between symmetric and asymmetric configurations is explained in terms of intermolecular steric interactions affecting the geometry relaxation of the precursor molecule after initial electron addition. For a quantitative assessment, the change in van der Waals energy resulting from elongation of the P–P bond of the molecules in their respective crystal lattices was calculated with X-ray crystallographic data. The calculations reveal significantly stronger steric interactions for the aromatic meso compounds than for their racemic forms, in agreement with the absence of P∴P σ^* configurations in the first. X irradiation of diphosphine disulfides in a frozen THF matrix almost invariably results in a single radical product, being the P∴P σ^* configuration, and differences between meso and racemic isomers disappear. This is a consequence of the fact that in a randomly oriented solid matrix the molecular packing is less tight than in a molecular crystal, making more space available to the precursor molecule. It is concluded that in case stabilization of the initial electron adduct via P–P bond length elongation is unfavorable because of steric interactions, other relaxation pathways become accessible, resulting in alternative phosphoranyl radical configurations.

In recent years the radiochemistry of organophosphorus compounds has received considerable attention. The phosphorus-centered radicals, formed in the radiation process, are of special interest because of their diverse structural and dynamical properties and their possible relevance to radiation damage in biochemical systems.[1-3] It has been shown from a number of single-crystal ESR studies that the precise nature of the configuration of a phosphoranyl radical depends on the type of ligands surrounding the central phosphorus nucleus. Only recently have effects other than the nature of the substituents been envisaged as being essential to the formation of radiogenic phosphorus-centered radicals. In this respect, aspects of conformation and configuration of the precursor molecules and the involvement of the precursor environment in the electron-capture process have been studied.[4-6]

Substituted diphosphine disulfides ($R_1R_2P(S)P(S)R_3R_4$) can serve as good probes to study phosphoranyl radical formation because of their intrinsic ability to adopt various radical configurations from a single molecule (Figure 1).[7] X irradiation of a diphosphine disulfide almost invariably results in the formation of an electron-capture radical in which the unpaired electron is accommodated in the antibonding σ^* orbital of the inter-phosphorus bond. As a consequence, the electron is symmetrically distributed over the two phosphorus nuclei. Complementary to this symmetrical P∴P σ^* configuration, several radical structures with an asymmetrical spin density distribution have been established. One of the asymmetric structures frequently observed is a radical in which the odd electron is located in the vacant equatorial position of a trigonal-bipyramidal configuration (TBP-*e*). Another asymmetric structure has been identified as a phosphoranyl radical in which the unpaired electron resides in an antibonding σ^* orbital of the phosphorus–sulfur bond (P∴S σ^*).

Table I. Numbering of Diphosphine Disulfide Derivatives

compd	stereo	R_1	R_2	R_3	R_4
1	meso	Me	Ph	Ph	Me
2	rac	Me	Ph	Me	Ph
3	meso	Me	Et	Et	Me
4	rac	Me	Et	Me	Et
5	meso	Me	*t*-Bu	*t*-Bu	Me
6	rac	Me	*t*-Bu	Me	*t*-Bu
7	meso	Me	*p*-Tol	*p*-Tol	Me
8	rac	Me	*p*-Tol	Me	*p*-Tol
9	meso	Ph	$PhCH_2$	$PhCH_2$	Ph
10	rac	Ph	$PhCH_2$	Ph	$PhCH_2$
11		Me	Ph	Ph	Ph
12		Me	Me	Ph	Ph

When different substituents ($R_1 \neq R_2$ and $R_3 \neq R_4$) are introduced into the diphosphine disulfide, the phosphorus atoms become chiral centers and the compounds may exist as diastereoisomers in meso and racemic forms. We have recently established that X irradiation of the meso and racemic forms of 1,2-dimethyl-1,2-diphenyldiphosphine disulfide (**1**, **2**) gives rise to completely different radical products.[4] The most striking dif-

† Eindhoven University of Technology.
‡ State University of Utrecht.

(1) Bentrude, W. G. *Acc. Chem. Res.* **1982**, *15*, 117.
(2) Tordo, P. *Landolt-Börnstein, New Series, Group II*; Fischer, H., Ed.; Springer-Verlag: Berlin, 1988; Vol. 17/e, pp 254–314, and references cited therein.
(3) Close, D. M. *Magn. Reson. Rev.* **1988**, *14*, 1, and references cited therein.
(4) Janssen, R. A. J.; van der Woerd, M. J.; Aagaard, O. M.; Buck, H. M. *J. Am. Chem. Soc.* **1988**, *110*, 6001.
(5) Aagaard, O. M.; Janssen, R. A. J.; de Waal, B. F. M.; Buck, H. M. *J. Am. Chem. Soc.* **1990**, *112*, 938.
(6) Cattani-Lorente, M.; Bernardinelli, G.; Geoffroy, M. *Helv. Chim. Acta* **1987**, *70*, 1897.
(7) Janssen, R. A. J.; Sonnemans, M. H. W.; Buck, H. M. *J. Chem. Phys.* **1986**, *84*, 3694.

0002-7863/90/1512-5432$02.50/0

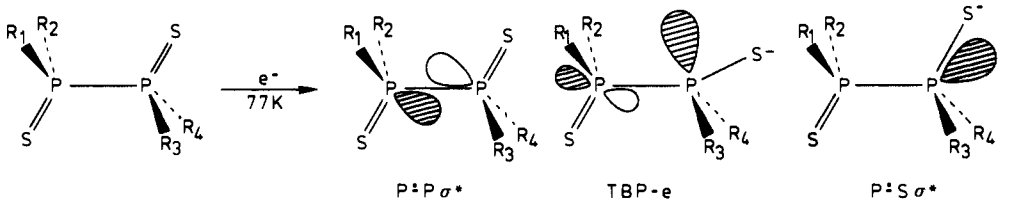

Figure 1. Formation of P∴P σ^*, TBP-*e*, and P∴S σ^* configuration by radiogenic electron capture of diphosphine disulfide derivatives.

ference observed is the absence of a symmetrical P∴P σ^* radical in the meso compound (**1**), because in all other X-irradiated diphosphine disulfides previously studied this configuration prevailed over the asymmetric structures.[7-9] This result would not be expected in advance because a P∴P σ^* molecular orbital can be accommodated perfectly by the initial C_i symmetry of the molecule. Moreover, quantum chemical calculations from a 4-31 G* basis set for *meso*- and *rac*-1,2-dimethyldiphosphine disulfide predict that the symmetrical P∴P σ^* structure is the most stable configuration for both isomers.[4] In order to illuminate this phenomenon, we performed extensive single-crystal, powder, and frozen-matrix ESR studies on the radiogenic electron-capture properties of several diastereoisomeric and asymmetric diphosphine disulfides (Table I) in which we concentrate on intrinsic and intermolecular effects on radical formation.

The choice of precursor molecules was based on several aspects. First, we were interested how radical formation of chiral *meso*- and *rac*-diphosphine disulfides is affected by the difference in the size of the substituents linked to the phosphorus nucleus. For this purpose, compounds **3–6** were studied. It is to be expected that if size difference effects would be important, substituting an ethyl group (**3**, **4**) by a bulky *tert*-butyl (**5**, **6**) should have a strong impact on the resulting radical products. Second, when the radiogenic behavior of compounds **7–10**, closely related to **1** and **2** are studied, the effect of aryl substituents directly linked to a phosphorus nucleus can be probed in more depth. Finally, compounds **11** and **12** were used to test the relevance of small symmetry distortions in discrimination between symmetrical and asymmetrical configurations. These two compounds possess an inherent asymmetry between the two phosphorus moieties, which possibly inhibits the formation of a symmetrical P∴P σ^* radical.

Aside from the aspects based on the intrinsic reactivity of the precursor, we examined the influence of intermolecular steric control[10-14] on the radiogenic behavior of the precursor molecules. For this reason all compounds were not only X irradiated in pure crystalline state but also, in case of sufficient solubility, embedded in a frozen tetrahydrofurane (THF) host matrix. Furthermore, the X-ray crystallographic structures of compounds **2**, **7**, and **8** were determined. In combination with the corresponding structures of **1**,[15] **5**,[16] and **6**,[16] we were able to calculate the change of the van der Waals energy in the crystal resulting from the geometry relaxation after formation of the initial electron-capture adduct.[5]

Our experiments show that the absence of a symmetrical P∴P σ^* configuration is an unique property of all meso compounds in which an aromatic substituent is directly linked to phosphorus. Even the asymmetric precursors **11** and **12** give rise to P∴P σ^* radical formation. The results are rationalized on the basis of the conformation of the precursor molecules in relation to their crystal environment. The van der Waals energy calculations demonstrate that in crystals of **1** and **7**, where no P∴P σ^* radical formation is detected, the elongation of the P–P bond is sterically more restricted than in **2**, **5**, **6**, and **8** in which the symmetrical radical configuration is readily formed. We conclude that P∴P σ^* radical formation is in general only possible on the condition that sufficient space is available for elongation of the original P–P bond in the crystal lattice. This provides new evidence for the fact that organic solid-state radiogenic reactions are topochemically controlled and tend to occur with minimum deforming of the surrounding crystalline matrix. Important support to this assertion comes from the fact that significant differences are established between X-irradiated diphosphine disulfides in crystalline solid state and in a THF host matrix.

Experimental Section

X Irradiation and ESR. Single crystals were glued onto a quartz rod and sealed in a quartz tube. A quartz tube containing a single crystal, powdered sample, or frozen solution was X irradiated in a glass Dewar vessel containing liquid nitrogen (77 K) with unfiltered radiation from a Cu source operating at 40 kV and 20 mA for 6–8 h. The ESR spectra were recorded on a Bruker ER 200D spectrometer, operating with an X-band standard cavity and interfaced with a Bruker Aspect 3000 computer. In a typical run the field sweep width of 0.1875 T was sampled with 4K data points, resulting in a digital resolution of 0.045 mT. The single crystals were rotated perpendicular to the magnetic field from 0 to 180°, in 10° steps, with a single-axis goniometer. The temperature was controlled with the aid of a Bruker ER 4111 variable-temperature unit.

Spectral Analysis. The *g* values and hyperfine coupling constants determined from the powder spectra were corrected with the Breit–Rabi equations.[17] The single-crystal spectra were analyzed with a computer program that calculates the spin Hamiltonian parameters from the angular dependences of the resonant fields. For the radicals studied, the spin Hamiltonian consists of Zeeman, nuclear Zeeman, and hyperfine parts of orthorhombic symmetry and noncoaxial orientation of **g** and **A**. The applied Hamiltonian is

$$\mathcal{H} = \beta \mathbf{S}\cdot\mathbf{g}\cdot\mathbf{H} - \sum_i g_{N,i}\beta_N \mathbf{I}_i\mathbf{H} + \sum_i \mathbf{S}\cdot\mathbf{A}_i\cdot\mathbf{I}_i$$

in which all symbols have their usual definitions. The program first determines the location of the ESR references axes throughout the rotational series. Then the initial **g** and **A** tensors are determined and subsequently corrected with the Breit–Rabi equations.[17] In a last step, the **g** and **A** tensors are adjusted to reproduce the observed field transitions for a number of special orientations. Finally, an accuracy test is performed in which the resonant fields are calculated via an exact diagonalization of the Hamiltonian with the final **g** and **A** tensors and compared to the observed values in order to obtain the rms error. Although the powder ESR spectra can be complex due to nonalignment of the **g** and hyperfine tensors and to the tensors not being perfectly axial, a close agreement is obtained between the principal values emerging from powder and single-crystal analyses. On the basis of this correspondence we expect the error in the powder data to be in the order of magnitude of the line width, i.e., approximately 1 mT (25 MHz).

X-ray Crystal Structure Analyses of 2, 7, and 8. For the three compounds cell parameters and crystal orientation parameters were obtained by least-squares refinement of the setting angles of 25 reflections ($25 < 2\theta < 41°$). The crystal of **2** showed considerable continuous decay during X-ray exposure. Therefore, the collection of data in half of the reflection sphere was repeated three times, and every 1 h three standard reflections were measured to monitor the decay process. In 36 h of X-ray exposure the intensities of the standard reflections dropped linearly to about 50% of the initial values. After correction for decay the rms deviation was less than 3%.

The data were corrected for Lorentz and polarization effects, but not for absorption. For compound **2** space group $P\bar{1}$ was confirmed by the

(8) Lyons, A. R.; Symons, M. C. R. *J. Chem. Soc., Faraday Trans. 2* **1972**, 1589.
(9) Claxton, T. A.; Fullam, B. W.; Platt, E.; Symons, M. C. R. *J. Chem. Soc., Dalton Trans.* **1975**, 1395.
(10) Schmidt, G. M. J. *Pure Appl. Chem.* **1971**, *27*, 647.
(11) Cohen, M. D. *Angew. Chem., Int. Ed. Engl.* **1975**, *14*, 386.
(12) Scheffer, J. R.; Trotter, J. *Rev. Chem. Intermed.* **1988**, *9*, 271.
(13) Ramamurthy, V.; Venkatesan, K. *Chem. Rev.* **1987**, *87*, 433.
(14) Zimmerman, H. E.; Zuraw, M. J. *J. Am. Chem. Soc.* **1989**, *111*, 7974.
(15) Wheatley, P. J. *J. Chem. Soc.* **1960**, 523. For van der Waals energy calculations hydrogen atoms were added with standard molecular parameters within C_i symmetry constraint.
(16) Wunderlich, H.; Wussow, H. G. *Z. Naturforsch.* **1984**, *39b*, 1581.
(17) Breit, G.; Rabi, I. I. *Phys. Rev.* **1931**, *38*, 2082.

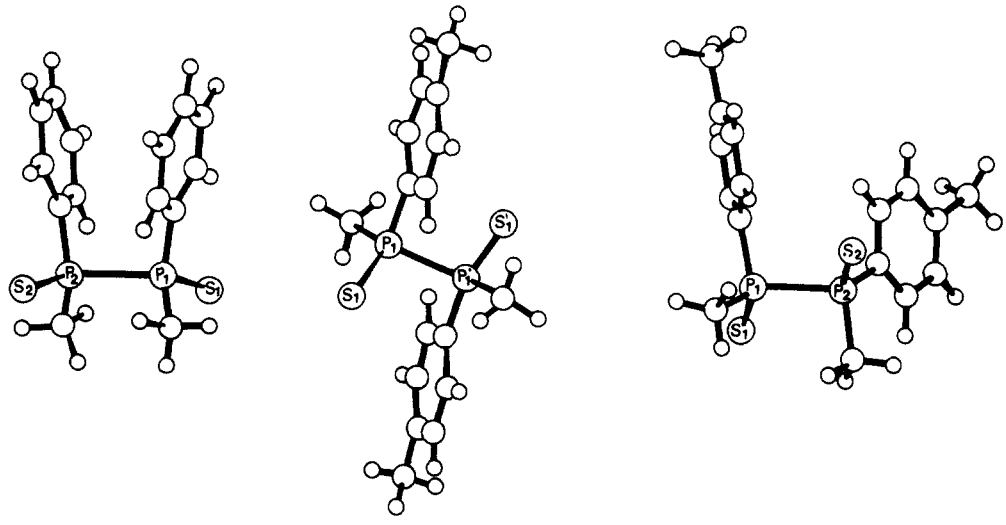

Figure 2. Molecular geometries of **2**, **7**, and **8** determined by crystallographic analysis.

results of the refinement. The space group extinctions for **7** ($0k0$ for $k = 2n + 1$ and $h0l$ for $h = 2n + 1$) indicate space group $P2_1/a$; for **8** the extinctions ($0k0$ for $k = 2n + 1$ and $h0l$ for $l = 2n + 1$) indicate space group $P2_1/c$. The structures were resolved by standard direct methods of SHELXS-86,[18] and the refinements were performed with SHELX-76.[19] The non-hydrogen atoms were refined anisotropically, and the hydrogen atoms were placed at calculated positions (C–H = 1.00 Å) and included in the refinement with general isotropic thermal parameters. The refinement weights were derived from counting statistics, and scattering factors were taken from ref 20. Table II contains the crystallographic data, data collection, and refinement details. Figure 2 shows the molecular geometries of **2**, **7**, and **8**. Tables of fractional atomic coordinates, thermal parameters, molecular geometries, and structure factor listings for **2**, **7**, and **8** are available on request.

Van der Waals Energy Calculations. The energy of steric interactions involved in the geometry relaxation after electron capture was calculated with the semiempirical potential function parametrized by Allinger et al.[21]

$$E_{vdw} = (\epsilon_i\epsilon_j)^{1/2}(1.84 \times 10^5 \exp(-12.0P) - 2.25P^6)$$

$$P = R_{ij}/(R_i^* + R_j^*)$$

in which ϵ_i is the energy parameter related to the depth of the potential well, R_i^* the van der Waals radius, and R_{ij} the internuclear distance. The P–P bond of the molecules was elongated, and the total change in E_{vdw} of an expanded crystal lattice was calculated for all atoms in the molecule. Allowance was made for the molecule to reorient by a change of the P–P bond direction.

Synthesis. Where necessary, experiments were done in an atmosphere of dry nitrogen. The solvents were dried by standard methods. NMR spectra were recorded on a Bruker AC 200 spectrometer at frequencies of 200.1 and 81.3 MHz for ^1H and ^{31}P, respectively. Chemical shifts are reported relative to TMS or a 85% aqueous H_3PO_4 solution (external standard), and downfield shifts are quoted positive. In all the NMR experiments we used $CDCl_3$ as solvent.

***meso*- and *rac*-1,2-dimethyl-1,2-diethyldiphosphine disulfide (3 and 4)** were synthesized according to the procedure described by Maier.[22] The meso compound **3** was readily obtained after recrystallization from ethanol. The racemic compound was purified by chromatography on a silica 60 column with chloroform as eluent (R_f(**3**) = 0.49, R_f(**4**) = 0.40), but due to a low yield of compound **4**, it could not be separated completely from **3** (3:4 ≡ 1:7.8). **3**: ^{31}P NMR δ 43.8; ^1H NMR δ 1.36 (6 H, dt, CCH_3), 1.89 (6 H, m, CH_3), 2.26 (4 H, m, CH_2C); mp 159–161 °C (lit.[22] mp 159–160 °C). **4**: ^{31}P NMR δ 44.1; ^1H NMR δ 1.29 (6 H, dt, CCH_3), 1.86 (6 H, m, CH_3), 2.12 (2 H, m, CH_2C), 2.35 (2 H, m, CH_2C); mp 98–99 °C (lit.[22] mp 103–104 °C).

***meso*- and *rac*-1,2-dimethyl-1,2-di-*tert*-butyldiphosphine disulfide (5 and 6)** were prepared according to a procedure reported by Hägele et al.[23]

Table II. Crystallographic Data, Data Collection, and Refinement Details for *rac*-1,2-Dimethyl-1,2-diphenyldiphosphine Disulfide (**2**), *meso*-1,2-Dimethyl-1,2-di-*p*-tolyldiphosphine Disulfide (**7**), and *rac*-1,2-Dimethyl-1,2-di-*p*-tolyldiphosphine Disulfide (**8**)

	2	**7**	**8**
	Crystal Parameters[a]		
formula	$C_{14}H_{16}P_2S_2$	$C_{16}H_{20}P_2S_2$	$C_{16}H_{20}P_2S_2$
fw	310.35	338.40	338.40
crystal system	triclinic	monoclinic	monoclinic
space group	$P\bar{1}$	$P2_1/a$	$P2_1/c$
a, Å	6.873 (1)	7.6520 (4)	12.2375 (7)
b, Å	9.052 (1)	12.2705 (5)	10.4163 (5)
c, Å	13.698 (3)	9.1212 (4)	14.0144 (7)
α, deg	94.50 (1)		
β, deg	91.85 (2)	92.102 (4)	94.960 (4)
γ, deg	112.05 (1)		
V, Å^3	785.7 (2)	855.85 (7)	1779.7 (2)
Z	2	2	4
D(calcd), g cm^{-3}	1.312	1.313	1.263
μ(Mo Kα), cm^{-1}	5.1	4.7	4.5
temp, K	295	295	295
crystal dimen, mm	0.30 × 0.10 × 0.05	0.40 × 0.25 × 0.02	0.40 × 0.20 × 0.03
	Data Collection		
diffractometer	Nonius-Enraf CAD 4		
radiation	Mo Kα		
wavelength, Å	0.71073		
scan type	$\omega - 2\theta$		
scan width, deg	0.60 + 0.35 tan θ	0.70 + 0.35 tan θ	0.65 + 0.35 tan θ
scan speed, deg min^{-1}	2.6	8.6	10.8
$2\theta_{max}$, deg	55.0	56.7	55.0
octants collected	$+h,\pm k,\pm l$	$-h,+k,\pm l$	$\pm h,+k,\pm l$
no. of reflcns collected	10646	2096	7594
no. of unique reflns	3605	1953	3927
R_{merge}, %	6.6	1.1	3.4
no. of obsd refln ($>2.5\sigma I$)	2648	1782	3143
no. of variables	164	92	182
	Refinement		
$R(F)$, %	9.2	3.5	3.5
$R(wF)$, %	9.3	3.9	3.6
goodness of fit (GOF)[b]	1.32	0.42	0.66
Δ/σ (mean)	0.0026	0.0088	0.0101
$\Delta(\rho)$, e Å^{-3}	0.86	0.47	0.29
N_o/N_v	16.1	19.4	17.3
std reflcns, h^{-1}	3	3	3
variation in stds, % rms	<3	<2	<2

[a] $R(F) = \sum(|F_o| - |F_c|)/\sum|F_o|$; $R(wF) = \sum(w^{1/2}(|F_o| - |F_c|))/\sum(w^{1/2}|F_o|)$. [b] GOF = $[\sum w(|F_o| - |F_c|)^2/(N_o - N_v)]^{1/2}$, $w = 1/\sigma_F^2$.

(18) Sheldrick, G. M. *SHELXS-86: A program for the solution of Crystal Structures from Diffraction Data*; Crystallographic Computing 3, Oxford University Press: Oxford, 1985; p 175.
(19) Sheldrick, G. M. *SHELX-76: A program for Crystal Structure Analysis*; Cambridge University: Cambridge, 1976.
(20) *International Tables for X-ray Crystallography*; Kynoch Press: Birmingham, 1974; Vol. IV (present distributor: D. Reidel; Dordrecht, The Netherlands).
(21) For sp^2 C and H: Allinger, N. L.; Lii, J.-H. *J. Comput. Chem.* **1987**, *8*, 1146. For sp^3 C, P, and S: Allinger, N. L.; Yuh, Y. H. MM2 program, QCPE 395.
(22) Maier, L. *Chem. Ber.* **1961**, *94*, 3043.

Table III. Spin Hamiltonian Parameters[a,b] for Powder and Host-Matrix ESR Experiments of Radicals Formed in Diphosphine Disulfide Derivatives

	P_1				P_2						
radical	$A_\perp$	$A_\parallel$	A_{iso}	$2A_{dip}$	$A_\perp$	$A_\parallel$	A_{iso}	$2A_{dip}$	$g_\perp$	$g_\parallel$	g_{iso}
3a	1287	1553	1383	170	1287	1553	1383	170	2.004	2.002	2.005
	1308				1308				2.008		
3a[c]	1224	1484	1311	173	1224	1484	1311	173	2.008	2.004	2.009
	1225				1225				2.014		
3b	1444	1785	1590	195	527	630	564	66	2.006	2.007	2.007
	1540				535				2.007		
3c	1517	1924	1653	271					2.011	1.997	2.006
3d	845	1303	998	305					2.017	2.003	2.012
4a	1283	1553	1380	173	1283	1553	1380	173	2.002	2.000	2.003
	1305				1305				2.008		
4a[c]	1209	1362	1260	102	1209	1362	1260	102	2.009	2.004	2.007
5a[c]	1245	1518	1336	182	1245	1518	1336	182	2.011	1.999	2.007
5c[c]	1288	1760	1445	315					2.013	2.002	2.009
6a[c]	1252	1529	1345	184	1252	1529	1345	184	2.013	1.999	2.008
6c[c]	1278	1751	1436	315					2.013	2.003	2.010
9a	1383	1960	1575	385					2.000	1.998	1.999
9b[c]	1171	1416	1254	162	1171	1416	1254	162	2.007	2.001	2.002
	1174				1174				1.997		
10a	1157	1404	1239	165	1157	1404	1239	165	2.007	2.000	2.005
10a[c]	1164	1386	1243	144	1164	1386	1243	144	2.016	2.003	2.006
	1177				1177				1.998		
10b[d]	1521	2072	1705	368					2.011	2.004	2.009
10c	1305	1635	1415	220					2.015	2.007	2.012
10d[c]	693	1122	836	286					2.017	2.003	2.012
11a[c]	1096	1408	1206	202	1096	1408	1206	202	2.001	2.000	2.004
	1115				1115				2.010		
11c[c]	669	1150	829	321					2.013	2.002	2.009
12a	1176	1396	1249	147	1176	1396	1254	147	2.017	2.003	2.012
12a[c]	1098	1371	1189	182	1098	1371	1189	182	2.006	2.001	2.004
12b	1281	1672	1412	261					2.012	2.002	2.009
12c	785	1264	931	332					2.014	2.002	2.010

[a] A in megahertz. [b] For a number of radicals two different perpendicular $A_\perp$ and $g_\perp$ values can be extracted from the ESR spectrum. [c] In THF host matrix. [d] Extra coupling of 65 MHz.

The individual meso and racemic compounds were obtained after chromatographing on a silica 60 column with *n*-hexane–diethyl ether as eluent (1:1 (v/v); R_f(**5**) = 0.35, R_f(**6**) = 0.50). Single crystals of both compounds were obtained by crystallization from ethanol. **5**: ^{31}P NMR δ 56.3; ^{1}H NMR δ 1.48 (18 H, m, $C(CH_3)_3$), 2.08 (6 H, d, CH_3, $^2J_{PCH}$ = 15.3 Hz); mp 143–144 °C (lit.[23] mp 141 °C). **6**: ^{31}P NMR δ 63.7; ^{1}H NMR δ 1.49 (18 H, m, $C(CH_3)_3$), 2.02 (6 H, d, CH_3, $^2J_{PCH}$ = 4.4 Hz); mp 115–116 °C (lit.[23] 118 °C).

***meso*- and *rac*-1,2-dimethyl-1,2-di-*p*-tolyldiphosphine disulfide (7 and 8)** were synthesized by a procedure analogous to that of Maier[22] with dichloromethylphosphine sulfide and *p*-tolylmagnesium bromide as reactants. Single crystals of **7** and **8** were obtained by crystallization from acetone and ethanol, respectively. **7**: ^{31}P NMR δ 36.4; ^{1}H NMR δ 1.92 (6 H, m, CH_3), 2.41 (6 H, s, $PhCH_3$), 7.32–7.40 (4 H, m, *m*-PhH), 7.95–8.08 (4 H, m, *o*-PhH); mp 215–216 °C. **8**: ^{31}P NMR δ 37.2; ^{1}H NMR δ 2.35 (6 H, m, CH_3), 2.36 (6 H, s, $PhCH_3$), 6.97–7.17 (4 H, m, *m*-PhH), 7.32–7.48 (4 H, m, *o*-PhH); mp 177–179 °C.

***meso*- and *rac*-1,2-dibenzyl-1,2-diphenyldiphosphine disulfide (9 and 10)** were prepared by a procedure analogous to that of Crofts and Gosling[24] with dichlorophenylphosphine sulfide and benzylmagnesium chloride as reactants. The meso component was obtained after recrystallization from chloroform; the racemic component, from several crystallizations from ethanol–ethyl acetate (5:1 (v/v)). **9**: ^{31}P NMR δ 40.8; ^{1}H NMR δ 3.28 (2 H, m, CHPh), 4.09 (2 H, m, CHPh), 6.90–7.08 (10 H, m, CPhH), 7.46–7.58 (6 H, m, *m*-PhH and *p*-PhH), 8.22–8.33 (4 H, m, *o*-PhH); mp 206–207 °C. **10**: ^{31}P NMR δ 42.8; ^{1}H NMR δ 3.82 (2 H, m, CHPh), 3.98 (2 H, m, CHPh), 7.12–7.25 (10 H, m, CPhH), 7.25–7.38 (6 H, m, *m*-PhH and *p*-PhH), 7.72–7.83 (4 H, m, *o*-PhH); mp 193–194 °C (lit.[24] mp 189.5–190.5 °C).

1-Methyl-1,2,2-triphenyldiphosphine disulfide (11) was synthesized by adding dropwise 0.81 g (0.0042 mol) of chloromethylphenylphosphine sulfide, which was prepared according to a literature procedure of Maier,[25] in 25 mL of dry toluene at room temperature to 0.93 g (0.0043 mol) of diphenylphosphine sulfide and 0.45 g of (0.0044 mol) triethylamine in 25 mL of dry toluene. After the mixture was stirred for 2 h, the solution was filtered, the solvent evaporated, and the crude reaction product chromatographed on a silica 60 column with *n*-hexane–diethyl ether (3:1 (v/v)) as eluent (R_f(**11**) = 0.50). After a second column chromatography with ethyl acetate–*n*-hexane (4:1 (v/v); R_f(**11**) = 0.40), the pure compound was obtained and crystallized from ethanol. **11**: ^{31}P NMR δ 37.5 (AB, $Ph_2P(S)$, J_{PP} = 25 Hz), 38.7 (AB, PhMeP(S)); ^{1}H NMR δ 2.30 (3 H, dd, CH_3, $^2J_{PCH}$ = 12.4 Hz, $^3J_{PPCH}$ = 6.7 Hz), 7.25–7.60 (9 H, m, *m*-PhH and *p*-PhH), 7.77–7.92 (4 H, m, *o*-PhH), 8.27–8.41 (2 H, m, *o*-PhH); mp 105–106 °C.

1,1-Dimethyl-2,2-diphenyldiphosphine disulfide (12) was prepared by adding dropwise 9.47 g (0.043 mol) of diphenylphosphine sulfide in 75 mL of dry toluene at room temperature to 5.58 g (0.043 mol) of dimethylchlorophosphine sulfide and 4.90 g (0.047 mol) of triethylamine in 100 mL of dry toluene and subsequent stirring for 2 h. The solution was filtered, and the solvent was evaporated. The crude reaction mixture was chromatographed on a silica 60 column with *n*-hexane–chloroform (1:1 (v/v); R_f(**12**) = 0.15). The pure compound was obtained by crystallization from ethanol. **12**: ^{31}P NMR δ 33.1 (d, $Ph_2P(S)$, J_{PP} = 23 Hz), 40.7 (d, $Me_2P(S)$); ^{1}H NMR δ 1.93 (6 H, dd, CH_3, $^2J_{PCH}$ = 12.3 Hz, $^3J_{PPCH}$ = 7.5 Hz), 7.50–7.60 (6 H, m, *m*-PhH and *p*-PhH), 8.30–8.40 (4 H, m, *o*-PhH); mp 108–109 °C (lit.[26] mp 112.7 °C).

Results and Assignment

***meso*-1,2-Dimethyl-1,2-diethyldiphosphine Disulfide (3).** The ESR powder spectrum of 8-h X-irradiated **3**, recorded at 105 K, reveals the characteristics of three different phosphoranyl-type radicals **3a–3c** (Figure 3a).

The spectrum of radical **3a** displays the three I = 1 (m_I = +1, 0, −1) lines of a triplet powder spectrum. The second central line (I = 0, m_I = 0) is hidden under the intense absorption lines of the irradiated quartz. The four-line pattern, resulting from the nondegeneracy of the m_I = 0 lines (second-order splitting), is caused by the large hyperfine interaction of the unpaired electron with two identical ^{31}P nuclei.[27] Radical **3b** displays the powder

(23) Hägele, G.; Tossing, G.; Kückelhaus, W.; Seega, J. *Z. Naturforsch.* **1984**, *39b*, 1574.
(24) Crofts, P. C.; Gosling, K. *J. Chem. Soc.* **1964**, 2486.
(25) Maier, L. *Helv. Chim. Acta* **1964**, *47*, 120.
(26) Koketsu, J.; Okamura, M.; Ishii, Y.; Goto, K.; Shimuzu, S. *Inorg. Nucl. Chem. Lett.* **1971**, *6*, 15.
(27) (a) Fessenden, R. W. *J. Chem. Phys.* **1962**, *37*, 747. (b) Fessenden, R. W.; Schuler, R. H. *J. Chem. Phys.* **1965**, *43*, 2704.

Table IV. Approximate Valence-Orbital Spin Densities for the Phosphorus-Centered Radicals Identified upon X Irradiation of Diphosphine Disulfide Derivatives 3–12

	P_1			P_2			
radical	ρ_s (%)	ρ_p (%)	p/s	ρ_s (%)	ρ_p (%)	p/s	total (%)
3a	10.3	23.2	2.25	10.3	23.2	2.25	67.0
3a[a]	9.8	23.6	2.41	9.8	23.6	2.41	66.8
3b	11.9	26.6	2.24	4.2	9.0	2.14	51.7
3c	12.4	37.0	2.98				49.4
3d	7.5	41.6	5.54				49.2
4a	10.3	23.5	2.28	10.3	23.5	2.28	67.4
4a[a]	9.4	13.9	1.48	9.4	13.9	1.48	46.6
5a	10.5	28.3	2.70	10.5	28.3	2.70	77.6
5a[a]	10.0	24.5	2.45	10.0	24.5	2.45	69.0
5b	11.5	23.9	2.08	6.1	24.8	4.07	66.3
5c	13.4	53.5	3.99				66.9
5c[a]	10.8	42.9	3.97				53.7
6a	10.7	30.5	2.85	10.7	30.5	2.85	82.4
6a[a]	10.7	25.1	2.35	10.7	25.1	2.35	71.6
6b	12.5	27.5	2.20	4.0	15.9	3.98	59.9
6c	11.8	44.1	3.74	0.9	4.2	4.67	61.0
6c[a]	10.8	42.9	3.97				53.7
6d	6.6	47.3	7.17				53.9
7a	12.7	51.3	4.04				64.0
8a(A)	9.8	23.1	2.36	9.8	23.1	2.36	65.8
8a(B)	10.0	25.6	2.56	10.0	25.6	2.56	71.2
8b	13.6	39.0	2.87	2.2	1.9	0.84	56.5
9a	11.8	53.4	4.53				65.2
9b[a]	9.4	22.1	2.35	9.4	22.1	2.35	63.0
10a	9.3	22.4	2.41	9.3	22.4	2.41	63.4
10a[a]	9.3	19.6	2.11	9.3	19.6	2.11	57.8
10b	12.7	50.1	3.94	4.6			67.4
10c	10.5	30.0	2.85				40.5
10d[a]	6.3	39.0	6.23				45.3
11a	9.5	23.1	2.43	9.5	23.1	2.43	65.2
11a[a]	9.0	27.5	3.06	9.0	27.5	3.06	73.0
11b	10.4	44.2	4.25	1.6	8.1	5.06	64.3
11c[a]	6.2	43.7	7.05				49.9
12a	9.3	20.0	2.14	9.3	20.0	2.14	58.6
12a[a]	8.9	24.8	2.79	8.9	24.8	2.79	67.4
12b	10.6	35.6	3.37				46.2
12c	7.0	45.2	6.46				52.2

[a] In THF host matrix.

spectrum associated with a double doublet arising from the coupling with two different ^{31}P nuclei. Radical **3c** results in a doublet powder spectrum in which hyperfine interaction with a single ^{31}P nucleus is presented. The parallel ($A_\parallel$) and perpendicular ($A_\perp$) parts of the hyperfine coupling constant and g values determined for **3a–3c** from the spectra are comprised in Table III along with the calculated isotropic (A_{iso}; $A_{iso} = (A_\parallel + 2A_\perp)/3$) and anisotropic or dipolar (A_{dip}; $A_{dip} = (A_\parallel - A_{iso})/2$) hyperfine constants. From A_{iso} and A_{dip} the valence s- and p-orbital spin densities are estimated (Table IV).[28]

On the basis of the hyperfine coupling with two identical ^{31}P nuclei, we attribute radical **3a** to a symmetrical P∴P σ^*-type radical. Moreover, the hyperfine couplings of **3a** are similar to symmetrical P∴P σ^*-type radicals previously generated in tetramethyl- and tetraethyldiphosphine disulfide.[7] On the basis of the different hyperfine interactions with two unequivalent ^{31}P nuclei, we attribute radical **3b** to a TBP-*e* configuration. This assignment is supported by the result that the parallel features of the largest coupling display perpendicular transitions of the smallest ^{31}P coupling. This is a consequence of the almost perpendicular orientation of their respective parallel principal directions, which indicates a TBP-*e* structure with a central ^{31}P nucleus and the contiguous ^{31}P nucleus in an axial position. The second axial position is occupied by the sulfur atom. The isotropic and dipolar hyperfine constants are again similar to TBP-*e* radicals generated in related diphosphine disulfide derivatives.[7] Radical **3c** is assigned to an asymmetrical three-electron-bond adduct between phosphorus and sulfur (P∴S σ^*), and its hyperfine data agree well with previous results.[7,29] When the X-irradiated sample is warmed, the signals diminish and are irreversibly lost at 230 K. Subsequently, a secondary phosphorus-centered radical appears (**3d**). This radical exhibits hyperfine interaction with one ^{31}P nucleus, and it is assigned to a dissociation product resulting from a rupture of the P–P linkage. A schematic representation of the observed radiogenic radical formation in **3** is depicted in Figure 4.

Interestingly, if **3** is X irradiated, being solvated in a frozen THF matrix, only the symmetrical P∴P σ^* radical can be detected (Figure 3b; Tables III and IV). This experiment demonstrates the decisive role of intermolecular geometrical considerations in controlling the course of the reaction. In the crystalline state with its packed three-dimensional periodic environment, a variety of products (**3a–3d**) is formed, whereas in a randomly oriented THF host matrix only one radical product is generated.

***rac*-1,2-Dimethyl-1,2-diethyldiphosphine Disulfide (4).** Due to a low yield of compound **4**, we could not purify it from **3** completely and a mixture (**3**:**4** ≡ 1:7.8) was used. After 8-h X irradiation, **4** displays the powder ESR spectrum depicted in Figure 5. From the spectrum we can assign radical **4a** with certainty. Other radicals, present in low concentration, could originate from **4** but cannot be identified unambigously because of interference of radicals generated in the impurity **3**.

Radical **4a** shows the same spectral features as radical **3a** and is therefore attributed to a P∴P σ^*-type radical (Figure 6).

If X irradiation of **4** is performed in a frozen THF matrix, the ESR spectrum is essentially identical with that of the crystalline compound, giving predominantly **4a**[30] (Tables III and IV).

(28) Morton, J. R.; Preston, K. F. *J. Magn. Reson.* **1978**, *30*, 577.

(29) (a) Janssen, R. A. J.; Kingma, J. A. J. M.; Buck, H. M. *J. Am. Chem. Soc.* **1988**, *110*, 3018. (b) Aagaard, O. M.; Janssen, R. A. J.; Buck, H. M. *Recl. Trav. Chim. Pays-Bas* **1989**, *108*, 262.

Table V. Hyperfine[a] and g Tensors[b] of Radicals **5a–5c**

radical	nucleus		total tensor	isotropic part	dipolar part	direction cosines x	y	z
5a		g	2.002			−0.932	0.181	0.314
			2.007	2.007		0.362	0.425	0.830
			2.014			−0.016	−0.887	0.462
	P_1, P_2	A	1294		−113	−0.444	−0.103	−0.890
			1313	1407	−94	0.117	0.978	−0.171
			1614		207	0.889	−0.180	−0.422
5b		g	2.003			0.999	−0.044	0.015
			2.006	2.006		−0.003	−0.373	−0.928
			2.010			−0.005	−0.927	0.372
	P_1	A	1418		−119	−0.954	−0.039	−0.298
			1481	1537	−56	0.067	0.938	−0.340
			1713		176	−0.293	0.344	0.892
	P_2	A	717		−97	−0.276	−0.045	−0.960
			727	814	−87	0.149	0.985	−0.089
			996		182	0.950	−0.167	−0.265
5c		g	2.000			−0.978	−0.096	0.184
			2.003	2.003		0.169	0.141	0.975
			2.004			−0.120	0.985	−0.122
	P_1	A	1589		−204	0.175	0.902	−0.394
			1605	1793	−188	0.172	−0.422	−0.890
			2186		393	0.970	−0.088	0.229

[a] A in megahertz. [b] The ESR reference x axis was chosen perpendicular to the plate face of the crystal; the other two, y and z, were chosen arbitrarily but were mutually orthogonal in the plane of the plate.

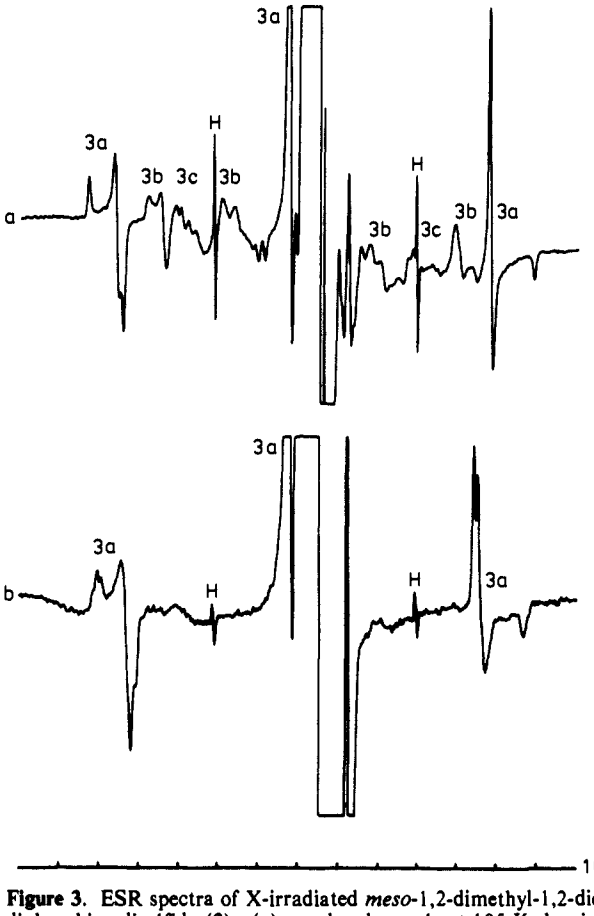

Figure 3. ESR spectra of X-irradiated *meso*-1,2-dimethyl-1,2-diethyldiphosphine disulfide (**3**): (a) powdered sample at 105 K showing the transitions of radicals **3a–3c**; (b) **3a** in a THF host matrix at 105 K.

Apparently, the symmetric P–P σ^* structure prevails in both diastereoisomeric forms (**3**, **4**) over asymmetric radical configurations and is the only phosphorus-centered radical formed when the compounds are enclosed by a THF host matrix.

Table VI. Relative Orientation (deg) of the Principal Directions[a] of the Hyperfine Couplings for Radicals Formed in **5**

radical	**5a**	**5b**$_1$	**5b**$_2$	**5c**
5a	0			
5b$_1$	45.7	0		
5b$_2$	9.7	55.1	0	
5c	38.7	96.3	29.0	0

[a] Because no absolute sign can be attributed to the direction of a principal value, there is an ambiguity of ±180° in the listed angles.

***meso*-1,2-Dimethyl-1,2-di-*tert*-butyldiphosphine Disulfide (5).** The X-ray crystallographic data of Wunderlich and Wussow[16] reveal that **5** crystallizes in the triclinic space group $P\bar{1}$ with 1 molecule in the unit cell (a = 6.765 Å, b = 7.788 Å, c = 8.060 Å, α = 73.29°, β = 64.94°, γ = 80.54°). The crystals are flat plates. After 6-h X irradiation, the ESR spectrum of a randomly oriented single crystal of **5** reveals the presence of three phosphoranyl-type radicals **5a–5c** (Figure 7).

The most intense absorptions, belonging to radical **5a**, constitute a four-line pattern and reveal hyperfine interaction with two identical ^{31}P nuclei. The central m_I = 0 lines are split as a result of the nondegeneracy of the I = 1 and I = 0 energy levels due to the large hyperfine interaction.[27] Radical **5b** shows hyperfine interaction with two different ^{31}P nuclei, resulting in a double doublet. Finally, radical **5c** displays hyperfine interaction with a single phosphorus atom resulting in a doublet.

In order to get detailed insight in the spin Hamiltonian parameters of these radicals, a full single-crystal ESR analysis was performed in which the X-irradiated crystal was rotated about three mutually orthogonal ESR reference axes. Throughout the rotations, each radical showed only one orientation in agreement with the crystallographic data (C_i symmetry, Z = 1).

The hyperfine and g tensors of radicals **5a–5c** and their isotropic and dipolar components, derived from the three principal values via the equations $A_{iso} = (A_1 + A_2 + A_3)/3$ and $A_{dip} = (A_3 - A_{iso})/2$, are given in Tables III and V, and the corresponding approximate valence s- and p-orbital spin densities are given in Table IV. Calculating the field transitions with the final g and A tensors yields a rms error of 0.16 mT that is substantially less than the line width of the absorptions.

Radical **5a** is assigned to a P–P σ^* structure since the hyperfine couplings are similar to radical **3a** (Figure 8). Radical **5b** is attributed to a TBP-*e* type radical with the adjacent phosphorus

(30) For radical **4a** generated in frozen THF the dipolar hyperfine coupling (102 MHz) emerging from the ESR spectrum is much less than the corresponding value for radical **4a** in crystalline solid state (173 MHz). The isotropic hyperfine couplings also deviate. This discrepancy is the result from the fact that the parallel features of **4a** are hardly discernable in the THF-host-matrix spectrum presumably due to the presence of a second unidentified radical product.

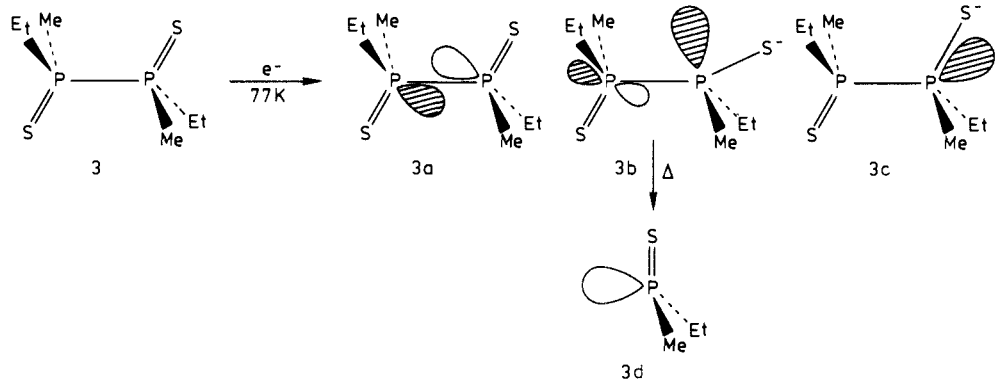

Figure 4. Structure of radicals **3a–3d** formed upon X irradiation of **3** and subsequent annealing.

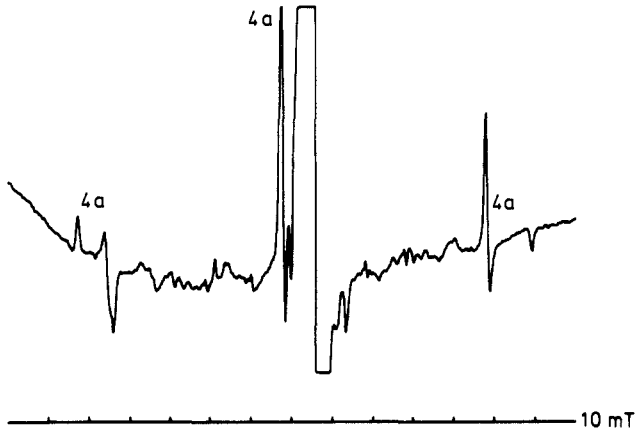

Figure 5. ESR powder spectrum of X-irradiated *rac*-1,2-dimethyl-1,2-diethyldiphosphine disulfide (**4**) at 105 K revealing the three $I = 1$ lines of radical **4a**.

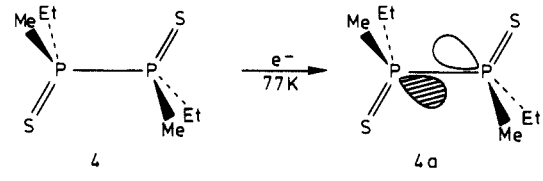

Figure 6. Structure of radical **4a** formed upon X irradiation of **4**.

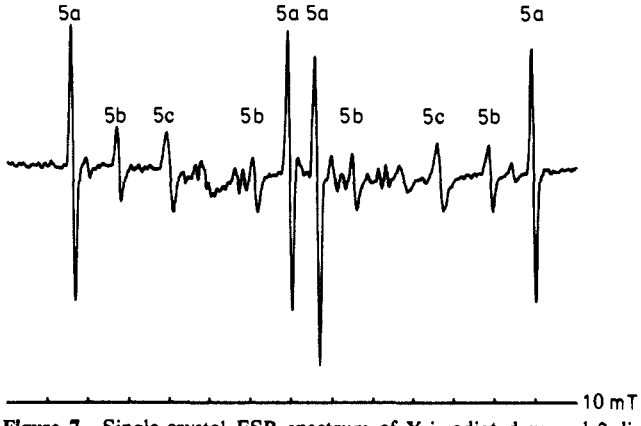

Figure 7. Single-crystal ESR spectrum of X-irradiated *meso*-1,2-dimethyl-1,2-di-*tert*-butyldiphosphine disulfide (**5**) showing the transitions of radicals **5a–5c** at 105 K.

atom and the sulfur atom in the axial positions. Radical **5c** is an asymmetrical P–S σ^*-type radical, and its spin Hamiltonian parameters are similar to those of the asymmetrical P–S σ^*-type radical formed in tetraethyldiphosphine disulfide.[7]

From the direction cosines of the largest principal hyperfine coupling, which correspond to the direction of the single occupied molecular orbital (SOMO), it is possible to calculate the relative orientations of the SOMOs of **5a–5c** (Table VI). It is readily shown that the directions of all the hyperfine couplings are coplanar. Single-crystal ESR experiments on tetramethyldiphosphine disulfide and ab initio quantum chemical calculations have shown that the principal direction of the SOMO of a symmetric P–P σ^* radical is located in the S–P–P–S plane and makes an angle of approximately 25–30° with the P–P bond.[7] Since all principal couplings of **5a–5c** are coplanar, a schematic representation of their SOMOs can be obtained by locating the directions in the S–P–P–S plane and fixing the angle of **5a** with the P–P bond to 25° (Figure 9).

The ESR spectrum of **5** in frozen THF is very different from the spectrum of the pure compound. Now two radical species could be identified, the P–P σ^* radical **5a** present in low concentration and the strong signals of a species comparable to radical **5c** but with a smaller contribution of the phosphorus valence s orbital (Tables III and IV).

Comparing the meso forms **5** and **3**, it appears that the radicals generated in the crystalline matrix are very similar, the only difference being the dissociation product, which is not detected in **5**. This leads to the suggestion that the *tert*-butyl group does not exert a large influence on the electron-capture behavior. Moreover, an absence of a P–P σ^*, as in the meso compound **1**, is not observed. Considering the bulkiness of the *tert*-butyl group, this leads to the imperative conclusion that the size of the substituents in itself is not the principal driving force for the observed discrimination between radiogenic radical configurations generated in *meso*- and *rac*-1,2-dimethyl-1,2-diphenyldiphosphine disulfide (**1** and **2**, respectively).

***rac*-1,2-Dimethyl-1,2-di-*tert*-butyldiphosphine Disulfide (6).** According to Wunderlich and Wussow,[16] **6** crystallizes in the monoclinic space group $P2_1$ with 2 molecules in the unit cell (a = 6.582 Å, b = 14.663 Å, c = 8.463 Å, β = 110.27°). The crystals obtained from ethanol are flat needles. The 2 molecules in the unit cell are of the same absolute configuration. The conformation of **6** is totally different from the one usually encountered for diphosphine disulfides; i.e., the bulky *tert*-butyl groups are trans-oriented and force the sulfur atoms into a gauche conformation. The crystal analysis, furthermore, reveals that the two phosphorus moieties of the molecule are slightly different, a fact

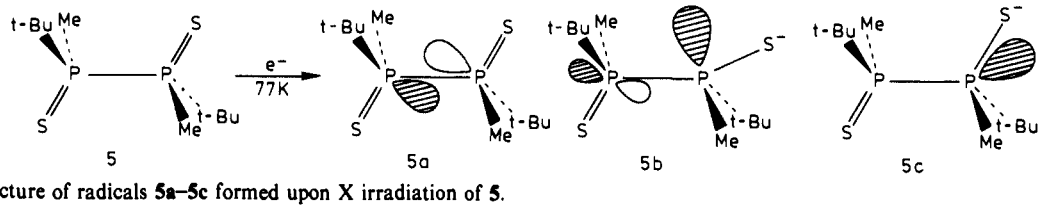

Figure 8. Structure of radicals **5a–5c** formed upon X irradiation of **5**.

Table VII. Hyperfine[a] and g Tensors[b] of Radicals **6a–6d**

radical	nucleus		total tensor	isotropic part	dipolar part	direction cosines x	y	z
6a		g	2.003			−0.526	0.224	−0.821
			2.008	2.008		−0.658	0.504	0.559
			2.012			0.539	0.834	−0.118
	P_1, P_2	A	1299		−124	0.567	−0.600	−0.563
			1325	1423	−98	0.620	0.762	−0.188
			1647		224	−0.542	0.242	−0.804
6b		g	2.003			−0.344	0.292	0.896
			2.004	2.005		0.706	0.706	0.049
			2.007			0.619	−0.649	0.442
	P_1	A	1552		−123	0.242	−0.132	0.961
			1596	1675	−79	−0.544	0.802	0.247
			1876		201	0.803	0.583	−0.122
	P_2	A	467		−67	−0.892	0.186	0.411
			487	534	−50	0.107	0.973	−0.206
			651		117	−0.438	−0.140	−0.888
6c		g	2.003			0.122	−0.061	0.991
			2.008	2.007		0.989	0.091	−0.116
			2.009			−0.083	0.994	0.071
	P_1	A	1399		−178	−0.757	0.485	−0.438
			1431	1577	−146	0.454	0.873	0.181
			1901		324	0.470	−0.062	−0.880
	P_2	A	100		−23	−0.989	−0.137	0.051
			115	123	−8	−0.134	0.990	0.045
			154		31	−0.057	0.037	−0.998
6d		g	2.002			−0.132	0.005	−0.991
			2.016	2.012		−0.986	−0.102	0.131
			2.017			−0.100	0.995	0.019
	P_1	A	702		−182	−0.979	0.049	0.196
			719	884	−165	0.048	0.999	−0.013
			1232		348	−0.196	−0.003	−0.981

[a] A in megahertz. [b] See text for definition of x, y, and z. The second orientation is related to (x,y,z) by $(\bar{x},y,\bar{z})$.

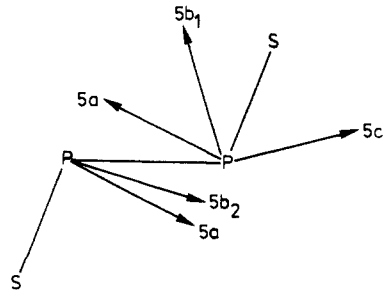

Figure 9. Schematic representation of the principal hyperfine coupling direction of **5a–5c** with respect to the molecular frame.

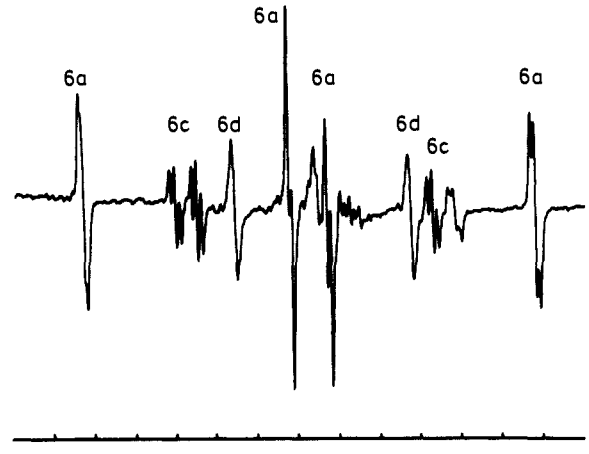

Figure 10. Single-crystal ESR spectrum of X-irradiated *rac*-1,2-dimethyl-1,2-di-*tert*-butyldiphosphine disulfide (**6**) showing the transitions of radicals **6a**, **6c** and **6d** at 120 K.

that has been confirmed by ^{31}P MAS solid-state NMR.[31]

The ESR spectrum of an X-irradiated, randomly oriented single crystal reveals the presence of two phosphoranyl type radicals (**6a** and **6b**) at low temperature (105 K). Slightly warming leads to a rapid loss of **6b** and the concurrent formation of two new phosphorus-centered radicals species (**6c** and **6d**) (Figure 10).

Radical **6a** displays an intense four-line pattern, where each line reveals an additional small hyperfine splitting (1.2 mT), probably resulting from hyperfine interaction with a ^1H nucleus. The spectrum of **6a** is readily associated with a radical possessing two identical ^{31}P nuclei. Radical **6b** gives rise to a double doublet as a result of the hyperfine interactions with two different ^{31}P nuclei. This radical is rather unstable and vanishes rapidly upon annealing. The ESR spectrum attributed to **6c**, which is a secondary radical, consists of four equally intense triplets. This complex pattern is the result of hyperfine interactions with two different ^{31}P nuclei and probably two identical ^1H atoms. The other secondary radical (**6d**) appears in the spectrum as a ^{31}P doublet.

Accurate spin Hamiltonian parameters were obtained from a single-crystal ESR analysis. The X-irradiated single crystal was rotated in three mutually orthogonal planes. For this purpose the x axis was chosen along the long needle axis, the y axis perpendicular to the flat needle face, and the z axis along the short needle axis. The orientation dependence of the resonant fields is depicted in Figure 11. A special feature that can be noted is the fact that in the xz plane only one orientation of every radical product is detected. This can be rationalized only when the y reference axis corresponds to the crystallographic b axis (2-fold screw axis). Magnetically inequivalent sites are observed for **6a** in the xy and yz planes and for **6b** in the xy plane.

The resonant field values were analyzed with the computer program, and the resulting hyperfine and g tensors are enumerated in Table VII. The corresponding valence-orbital spin densities are listed in Table IV. The rms error of the calculated field transitions, averaged over the different radical species, amounts to 0.25 mT.

The assignment of **6a–6d** to specific radical structures is not straightforward and will be elaborated in some detail. The most

(31) Harris, R. K.; Merwin, L. H.; Hägele, G. *J. Chem. Soc., Faraday Trans. 1* **1987**, *83*, 1055.

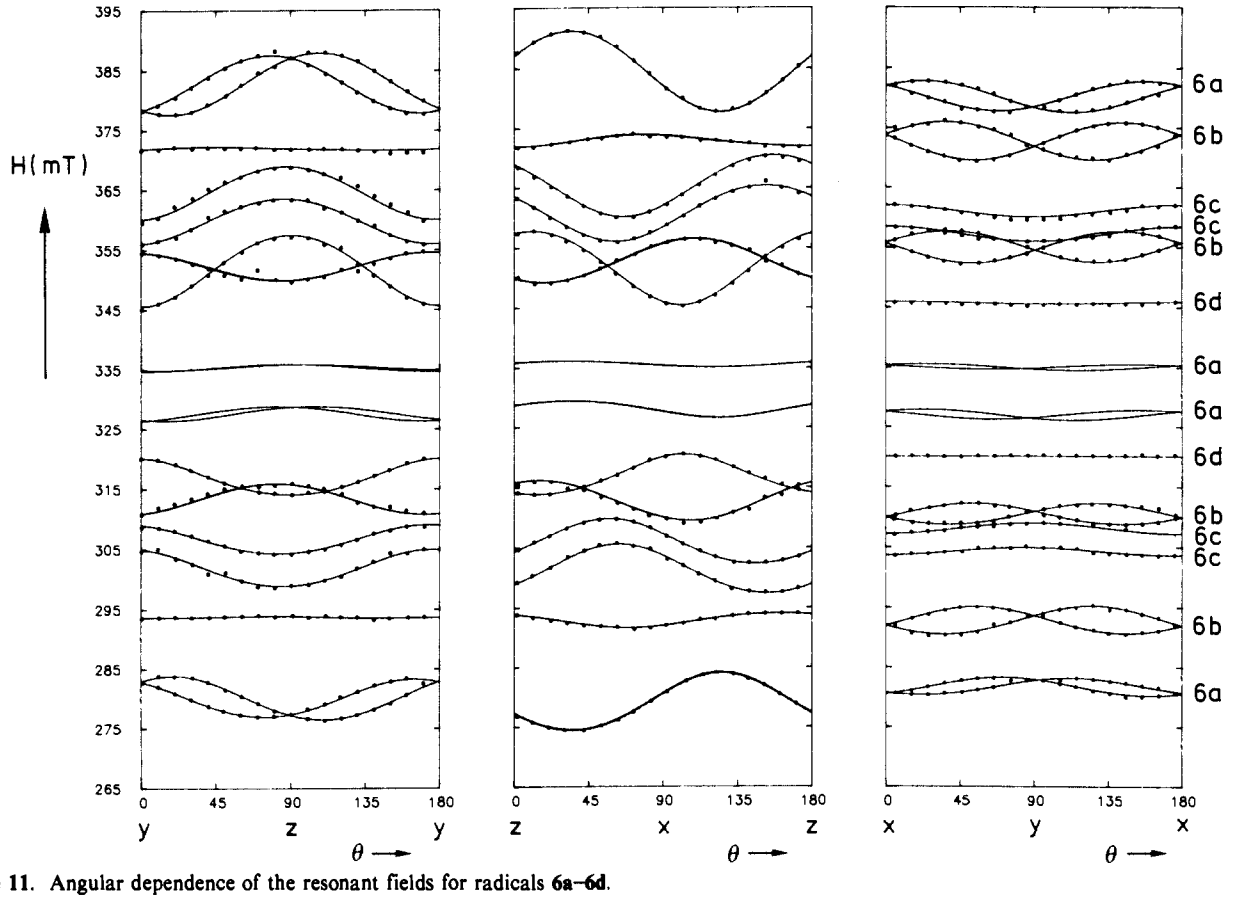

Figure 11. Angular dependence of the resonant fields for radicals **6a–6d**.

plausible inference of the result that radical **6a** possesses two identical phosphorus nuclei is that **6a** represents a symmetrical P–P σ^* configuration. Since the hyperfine couplings of the two ^{31}P nuclei appear to be equivalent for all orientations of the magnetic field,[32] the principal directions of the hyperfine tensors must coincide. As a consequence of the near C_2 symmetry of the precursor molecule, these principal directions must either coincide with or else be perpendicular to the C_2 axis. The SOMO of the P–P σ^* radical must, therefore, be located in the *t*-Bu–P–P–*t*-Bu plane, which also accounts for the high total spin density on the two phosphorus atoms (82.4%) due to a decreased spin delocalization onto the adjacent sulfur atoms. Radical **6b** is attributed to a TBP-*e* type radical with the neighboring phosphorus and sulfur atoms in the axial positions. The spin Hamiltonian parameters of **6b** are similar to those of radical **3b**. Radical **6c** is assigned to an asymmetric P–S σ^*-type radical with a small hyperfine coupling from the second phosphorus nucleus.[33] Radical **6d** is a dissociation product resulting from a rupture of the P–P linkage. A careful evaluation of the direction cosines and the total number of observed magnetically inequivalent sites of **6b–6d** reveals that each of these radical species, in which the unpaired electron is primarily localized on one half of the molecule, must descend from only one of the two geometrically nonidentical phosphorus moieties

Table VIII. Relative Orientation (deg) of the Principal Directions[a] of the Hyperfine Couplings for Radicals Formed in **6**

radical	6a	$6b_1$	$6b_2$	$6c_1$	$6c_2$	6d
6a	0					
$6b_1$	88.7	0				
$6b_2$	23.3	109.3	0			
$6c_1$	64.0	63.3	54.3	0		
$6c_2$	32.6	84.4	25.1	31.8	0	
6d	47.0	92.3	16.9	39.5	8.2	0

[a] Because no absolute sign can be attributed to the direction of a principal value, there is an ambiguity of ±180° in the listed angles.

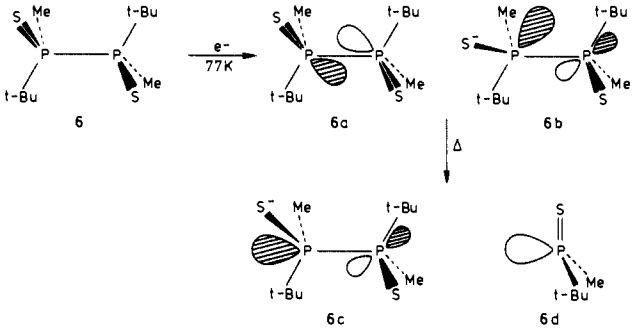

Figure 12. Structure of radicals **6a–6d** formed upon X irradiation of **6** and subsequent annealing.

present in the molecule (e.g., the TBP-*e* radical **6b** cannot be generated in one molecule on P_1 and in another molecule on P_2). This interesting effect emphasizes the complexity of factors involved in the formation of electron-capture products.

The relative orientations of the SOMOs calculated from the direction cosines of the largest hyperfine coupling constants are given in Table VIII. A schematic representation of the radical structures is depicted in Figure 12.

We also studied the radiogenic radical formation of **6** in a THF host matrix. X irradiation results in an ESR spectrum that is

(32) It is difficult to prove the exact equivalence of the two ^{31}P nuclei for all orientations, since it is not always possible to distinguish between the ESR spectra of two identical nuclei and two nuclei with slightly different couplings. As an example, consider the isotropic ^{31}P hyperfine couplings A_1 and A_2 of a hypothetical radical with $g = 2.00232$ and a spectrometer frequency of 9.4 GHz (X band). In the case $A_1 = A_2 = 1000$ MHz, exact diagonalization of the appropriate spin Hamiltonian leads to four absorptions at 297.73, 331.59, 335.42, and 369.30 mT. If A_1 and A_2 are not exactly equivalent, e.g., $A_1 = 1050$ MHz and $A_2 = 950$ MHz, similar field transitions are obtained: 297.73, 330.87, 336.12, and 369.30 mT. It appears that the outmost transitions remain unaltered whereas the central lines shift approximately 0.7 mT, which is much less than predicted by first-order perturbation theory (1.8 mT ≡ 50 MHz).

(33) An alternative assignment for this species would be a distorted TBP structure with the second phosphorus occupying the equatorial position. This configuration would explain the observed additional ^{31}P hyperfine coupling but implies on the other hand an axial position of a carbon atom in the TBP, which is less probable.

Table IX. Hyperfine and g Tensors[b] of Radical **7a**

radical	nucleus		total tensor	isotropic part	dipolar part	direction cosines		
						x	*y*	*z*
7a		g	1.997			0.768	0.214	0.604
			1.999	1.999		0.238	−0.970	0.040
			2.000			−0.595	−0.133	0.796
	P_1	A	1487		−205	0.537	0.307	−0.786
			1521	1692	−171	−0.102	0.948	0.301
			2069		377	0.838	−0.081	0.540

[a] A in megahertz. [b] The *x* axis is located perpendicular to the flat lozenge-shaped face of the crystal; the *y* and *z* axes were chosen along the diagonals of the lozenge.

Figure 13. Single-crystal ESR spectrum of X-irradiated *meso*-1,2-dimethyl-1,2-di-*p*-tolyldiphosphine disulfide (**7**) showing the transitions of radical **7a** at 105 K.

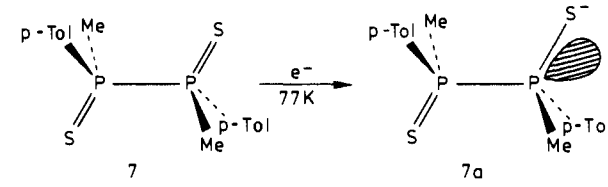

Figure 14. Structure of radical **7a** formed upon X irradiation of **7**.

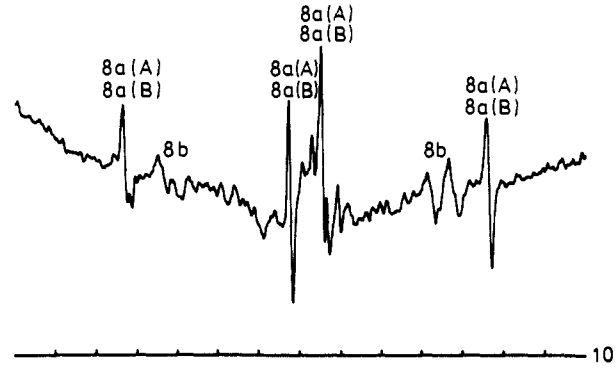

Figure 15. Single-crystal ESR spectrum of X-irradiated *rac*-1,2-dimethyl-1,2-di-*p*-tolyldiphosphine disulfide (**8**) showing the transitions of radicals **8a** and **8b** at 105 K.

essentially identical with that of its meso isomer, **5**, and hence similar radicals must have been formed. They are assigned to P–P σ^* (**6a**) and P–S σ^* (**6c**) structures (Tables III and IV). It is to be noted that compounds **5** and **6**, when X irradiated in a THF host matrix, react in a manner different from all other diphosphine disulfides by the fact that the P–P σ^* configuration is not the most abundant electron-capture product, but instead the P–S σ^* configuration prevails.

***meso*-1,2-Dimethyl-1,2-di-*p*-tolyldiphosphine Disulfide (7).** The meso isomer **7** is crystallized from acetone. X-ray crystallographic analysis (Table II) reveals a $P2_1/a$ space group with 2 molecules of C_i symmetry with centers at (0, 0, $^1/_2$) and ($^1/_2$, $^1/_2$, $^1/_2$) in the unit cell (a = 7.6520 Å, b = 12.2705 Å, c = 9.1212 Å, β = 92.102°). The molecules possess a P–P bond length of 2.2309 (6) Å and a trans conformation of the two sulfur nuclei. The bond distances and angles are in agreement with other known diphosphine disulfides.[15,16,34-36]

The ESR spectrum of a randomly oriented, X-irradiated single crystal of **7** shows the weak features of a single phosphoranyl-type radical **7a** (Figure 13). The ESR absorptions of **7a** constitute a doublet, indicating hyperfine interaction with one ^{31}P nucleus. Upon warming, no new radical species can be detected and **7a** is irreversibly lost at 250 K.

On the basis of $P2_1/a$ symmetry of the crystal, two magnetically different orientations of **7a** can be expected. The fact that during rotation of the crystal in three mutual orthogonal planes only one orientation is observed can be rationalized with either an orthogonal or parallel orientation of the SOMO with the 2-fold crystallographic screw axis (b axis). The results of the single-crystal ESR analysis are given in Table IX. The y component of the eigenvector corresponding to the largest principal hyperfine coupling amounts to only −0.081, suggesting that the SOMO is orthogonal to b. The 2-fold symmetry transfers a SOMO in the (x,0,z) direction to the magnetically equivalent direction ($\bar{x}$,0,$\bar{z}$). The rms error of the calculated field transitions is 0.17 mT, substantially less than the line width.

We assign **7a** to an asymmetrical P–S σ^*-type radical (Figure 14). The spin Hamiltonian parameters are similar to those of previously reported P–S σ^* radicals.[7,29] The very low solubility of **7** in etheric solvents precluded a host-matrix study.

Summarizing, it appears that, analogous to **1**, no symmetrical P–P σ^* configuration is formed in this meso form after X irradiation.

***rac*-1,2-Dimethyl-1,2-di-*p*-tolyldiphosphine Disulfide (8).** Single crystals of **8** are obtained by crystallization from ethanol. The crystallographic analysis (Table II) reveals a monoclinic $P2_1/c$ space group with 4 molecules in the unit cell (a = 12.2375 Å, b = 10.4163 Å, c = 14.0144 Å, β = 94.960°). This compound crystallizes as a racemic form containing both R,R and S,S molecules. The asymmetric unit in the cell is one entire molecule. The molecules possess no internal symmetry element, the P–P bond distance is 2.2259 (8) Å, and the SPPS torsion angle amounts to 176.34 (4)°, indicating a small deviation from an exact trans location. The halves of the molecules differ mainly by the orientation of the *p*-tolyl group with respect to the P–P bond (PPCC torsion angles of 112.9 (2)° and 77.9 (2)°).

X irradiation of **8** results in an ESR spectrum in which two types of phosphoranyl radicals can be detected, **8a** and **8b** (Figure 15).

The most intense absorptions (**8a**) form a four-line pattern from which hyperfine interactions with two identical ^{31}P nuclei can be deduced. Radical **8b** exhibits a double doublet pattern indicating hyperfine interaction with two different ^{31}P atoms.

In order to obtain better insight into the orientational dependence of the hyperfine and **g** tensors, a full single-crystal ESR analysis was performed. Prior to the automated calculation of the spin Hamiltonian parameters, radical **8a** seemed to be present in four orientations and radical **8b** in two, but the computations reveal that the spectrum of radical **8a** constitutes in fact two orientations of two slightly different P–P σ^* radicals, **8a**(A) and **8a**(B) (Table X). Radical **8b** is attributed to an asymmetrical P–S σ^*-type radical having a small hyperfine interaction with

(34) Blake, A. J.; Howie, R. A.; McQuillan, G. P. *Acta Crystallogr.* **1981**, *B37*, 966.
(35) Lee, J. D.; Goodacre, G. W. *Acta Crystallogr.* **1971**, *B27*, 307.
(36) Dutta, S. N.; Woolfson, M. M. *Acta Crystallogr.* **1961**, *14*, 178.

Table X. Hyperfine[a] and g Tensors[b] of Radicals 8a(A), 8a(B), and 8b

radical	nucleus		total tensor	isotropic part	dipolar part	direction cosines x	y	z
8a(A)		g	2.000			-0.681	-0.567	-0.463
			2.004	2.004		0.532	-0.818	0.219
			2.009			-0.503	-0.098	0.859
	P_1, P_2	A	1201		-101	0.331	-0.938	0.098
			1234	1302	-68	0.492	0.084	-0.867
			1471		169	-0.805	-0.335	-0.489
8a(B)		g	1.999			-0.445	-0.763	-0.470
			2.004	2.004		0.850	-0.525	0.047
			2.009			-0.282	-0.378	0.882
	P_1, P_2	A	1225		-115	0.903	-0.397	-0.164
			1266	1340	-74	0.066	0.504	-0.861
			1527		187	-0.424	-0.767	-0.481
8b		g	2.002			-0.179	0.676	0.715
			2.009	2.009		0.973	0.231	0.025
			2.016			0.148	-0.700	0.699
	P_1	A	1648		-173	0.259	0.736	0.626
			1708	1821	-113	0.234	-0.676	0.699
			2107		286	-0.937	0.035	0.347
	P_2	A	18		-11	0.509	-0.622	0.595
			26	29	-3	-0.815	-0.125	0.566
			42		14	-0.278	-0.773	-0.571

[a] A in megahertz. [b] The three ESR reference axes (x,y,z) were arbitrarily but mutual orthogonal.

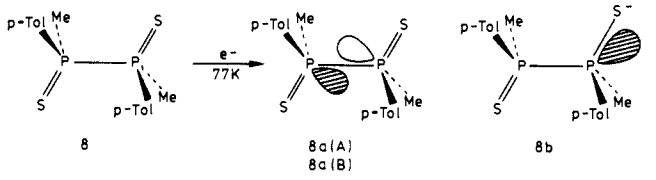

Figure 16. Structure of radicals 8a(A,B) and 8b formed upon X irradiation of 8.

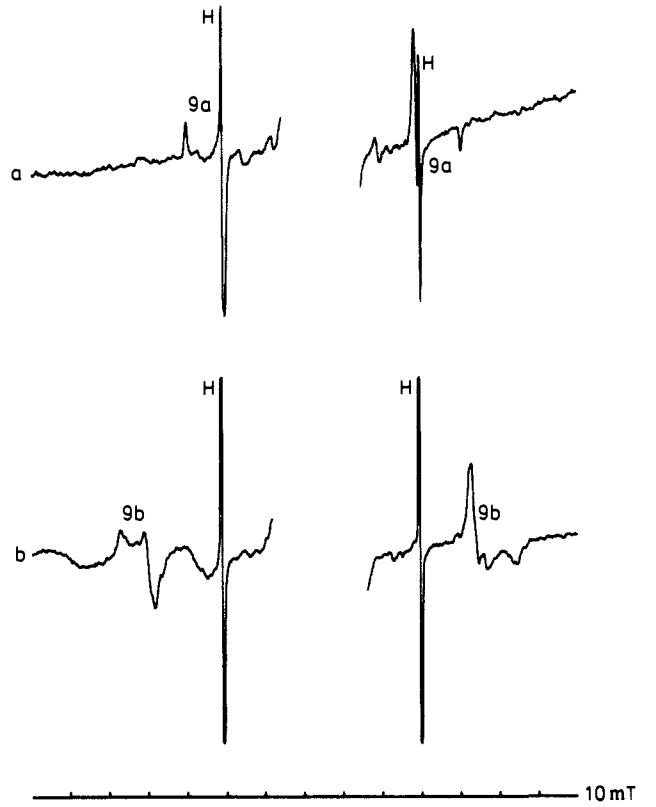

Figure 17. ESR spectra of X-irradiated *meso*-1,2-dibenzyl-1,2-diphenyldiphosphine disulfide (9): (a) powdered sample showing the transitions of 9a at 105 K; (b) 9b in a THF host matrix at 105 K.

the neighboring phosphorus atom.[33] The rms error of the calculated field transitions amounts to 0.27 mT. Table XI shows the relative orientations of the direction of the SOMOs. The fact

Table XI. Relative Orientation (deg) of the Principal Directions[a] of the Hyperfine Couplings for Radicals Formed in 8

radical	8a(A)	8a(B)	$8b_1$	$8b_2$
8a(A)	0			
8a(B)	35.2	0		
$8b_1$	52.0	75.6	0	
$8b_2$	57.1	26.2	78.2	0

[a] Because no absolute sign can be attributed to the direction of a principal value, there is an ambiguity of ±180° in the listed angles.

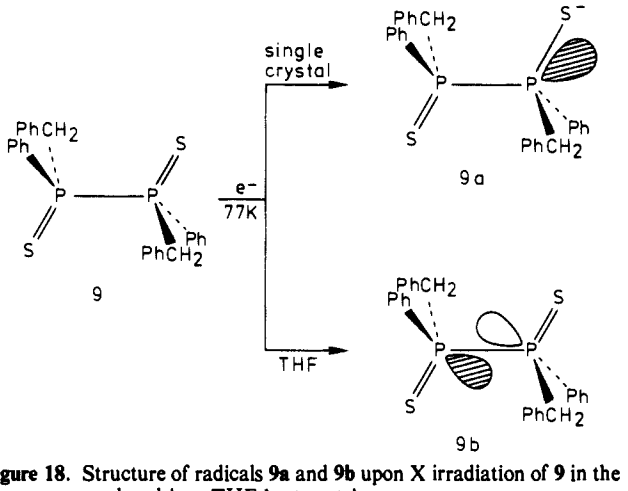

Figure 18. Structure of radicals 9a and 9b upon X irradiation of 9 in the pure compound and in a THF host matrix.

that radicals 8a(A), 8a(B), and 8b are present in two orientations is in accord with the symmetry of the $P2_1/c$ space group in which the four molecules occupy two sets of magnetically unequivalent orientations ((x,y,z), and ($\bar{x}$,y,$\bar{z}$)). No experiments in a THF host matrix were done for 8, because a comparison with the corresponding meso structure (7) is not possible (vide supra).

Figure 16 gives a schematic representation of the radical precursor and radical formation.

***meso*-1,2-Dibenzyl-1,2-diphenyldiphosphine Disulfide (9).** The ESR powder spectrum of an X-irradiated sample of 9, recorded at 105 K, reveals the features of a single phosphoranyl-type radical 9a (Figure 17a).

Radical 9a gives the powder pattern of a doublet exhibiting hyperfine interaction with one ^{31}P nucleus. The spin Hamiltonian parameters and corresponding orbital spin densities are given in Tables III and IV. We assign radical 9a to an asymmetrical P–S

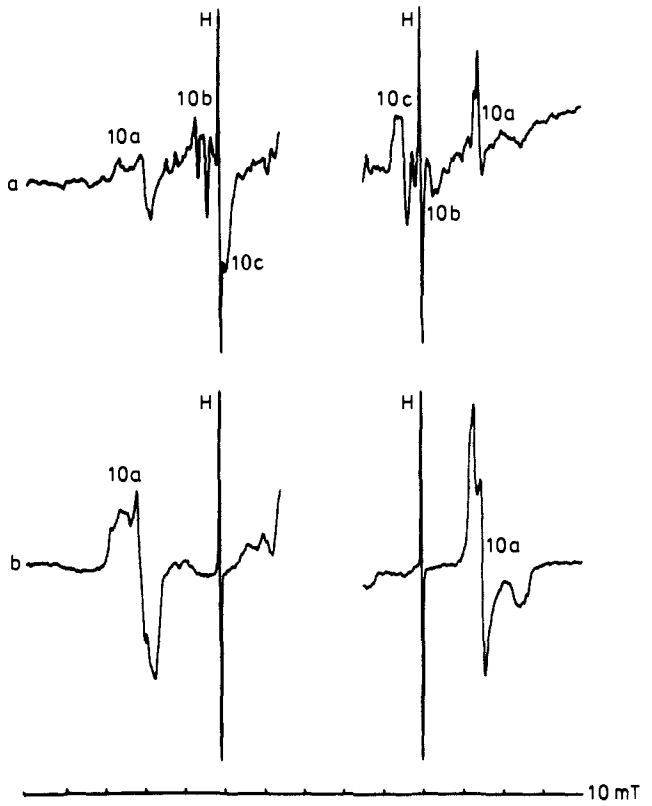

Figure 19. ESR spectra of X-irradiated *rac*-1,2-dibenzyl-1,2-diphenyldiphosphine disulfide (**10**): (a) powdered sample at 105 K showing the transitions of radicals **10a–10c**; (b) **10a** in a THF host matrix at 105 K.

σ^*-type radical (Figure 18). Again the presence of an aryl group linked to phosphorus leads to the absence of the symmetrical P–P σ^* radical in the meso form. Upon warming, no new phosphoranyl radical is formed and radical **9a** is irreversibly lost at 250 K.

In contrast to the meso compounds **1** and **7**, **9** is readily soluble in etheric solvents, giving the opportunity to study its electron-capture behavior in host-matrix environments. X irradiation of **9** in a THF matrix results in radical species **9b**, which is completely different from the crystalline-state product **9a** (Figure 17b). Now the spectral features indicate hyperfine interaction with two identical ^{31}P atoms, and we assign radical **9b** to a symmetrical P–P σ^*-type radical (spin Hamiltonian and approximate orbital spin densities are given in Tables III and IV). Radical **9b** is rapidly lost upon annealing, and no new phosphorus-centered radicals are detected.

***rac*-1,2-Dibenzyl-1,2-diphenyldiphosphine Disulfide (10).** After X irradiation of **10** the ESR powder spectrum reveals the features of at least three phosphoranyl-type radicals (**10a–10c**) (Figure 19a).

Upon warming, radical **10a** decreases rapidly and is irreversibly lost at 135 K. Further annealing leads to the loss of **10b** at 145 K. Radical **10c** is lost at 215 K, and no new phosphorus-centered radical species appear. The spin Hamiltonian parameters and corresponding valence-orbital spin densities are enumerated in Tables III and IV. The spectral features of radical **10a** indicate hyperfine interaction with two identical ^{31}P nuclei from which we conclude that **10a** is a P–P σ^*-type radical. Radical **10b** displays the powder pattern of an asymmetrical P–S σ^*-type radical having a large hyperfine interaction with one ^{31}P atom and a small, nearly isotropic, hyperfine interaction with another $I = {}^1/_2$ nucleus (possibly a ^1H atom or the adjacent ^{31}P atom). Radical species **10c**, the most intense and most stable radical configuration, exhibits a doublet powder spectrum indicating hyperfine interaction with only one ^{31}P nucleus. We assign **10c** to an alternative configuration of an asymmetrical P–S σ^*-type radical (Figure 20).

X irradiation of **10**, dissolved in a THF matrix, yields the same spectral features as radical **9b**, so again only the symmetrical P–P

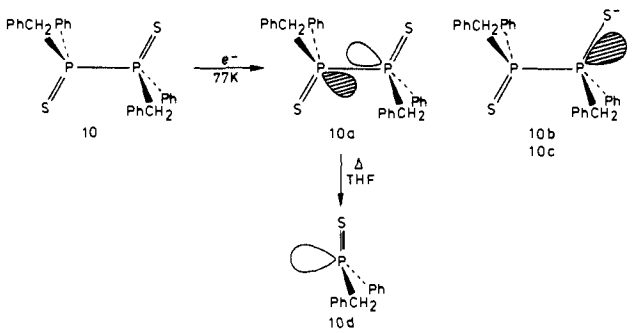

Figure 20. Structure of radicals **10a–10d** formed upon X irradiation of **10**.

σ^*-type radical (**10a**) is formed (Figure 19b). When the temperature is slowly raised, the signals of **10a** are lost and a thiophosphonyl radical (**10d**) is formed as a result of a rupture of the P–P bond.

Apparently, the differences between compounds **9** and **10** in the X-irradiated crystal solid state have disappeared in the THF host matrix. The difference between radiogenic radical formation in the crystalline and host-matrix experiments must originate either from the influence of the crystal lattice or from a completely different conformation of the aryl ligands or from a combination of both. It is clear that the radiogenic behavior of the diastereoisomeric molecules changes dramatically by removing the molecule from its crystal environment and placing it in the THF host matrix. The absence of radicals **10b** and **10c** in the THF host matrix indicates that by offering enough space to the radical precursor to change its geometry after electron capture, only the thermodynamically most stable radical, being the P–P σ^* configuration, will be formed ultimately leading to dissociation when the temperature is raised. The diversity of radicals formed in the solid crystal state must therefore originate from the strong impact of the lattice on the kinetics of the P–P σ^* formation by which secondary reactions can occur.[37]

1-Methyl-1,2,2-triphenyldiphosphine Disulfide (11). Compound **11** was crystallized from ethanol, and a single crystal, shaped as a tetragonal prism, was X-irradiated for 8-h. The ESR spectrum at 105 K of this randomly oriented single crystal shows the absorptions of three phosphoranyl-type radicals of which only two could be assigned with certainty, **11a** and **11b** (Figure 21a).

Upon annealing, **11a** is readily lost at 145 K. Concurrently there is a small increase of the unassigned radical (indicated in Figure 21a with an asterisk). Further warming does not result in new radical configurations, and all phosphoranyl radicals are irreversibly lost at 245 K.

The hyperfine and **g** tensors were obtained by performing a single-crystal ESR analysis (Tables XII and XIII). The computer program yields a rms error of 0.17 mT for the calculated field transitions.

Radical **11a** is attributed to a symmetrical P–P σ^* configuration that is formed in spite of the fact that the precursor possesses two completely different phosphorus nuclei. Radical **11b** can be assigned to an asymmetrical P–S σ^*-type radical, in which the extra coupling comes from the neighboring phosphorus atom (Figure 22).[33] The isotropic and anisotropic hyperfine coupling constants of P_1 in **11b** have a close resemblance to those of the asymmetrical P–S σ^*-type radical formed in **1**.[4] It is reasonable to assume that the main spin density of the unpaired electron resides at the MePhP(S) moiety of the molecule.

Like the other compounds, we also studied the electron-capture properties of **11** embedded in frozen THF. The resulting ESR spectrum (Figure 21b) clearly shows the formation of the P–P σ^* radical **11a** and the concurrent absence of P–S σ^* or TBP-*e* configurations. The only asymmetric phosphorus-centered radical detected in a dissociation product **11c** whose concentration in-

(37) Zimmerman, H. E.; Zuraw, M. J. *J. Am. Chem. Soc.* **1989**, *111*, 2358.

Table XII. Hyperfine[a] and g Tensors[b] of Radicals **11a** and **11b**

radical	nucleus		total tensor	isotropic part	dipolar part	direction cosines x	y	z
11a		g	2.000			0.032	0.999	−0.025
			2.006	2.005		0.613	0.000	0.790
			2.009			−0.790	0.041	0.612
	P_1, P_2	A	1175		−87	−0.032	0.202	−0.979
			1179	1262	−83	0.989	0.150	−0.001
			1432		170	0.146	−0.968	−0.205
11b		g	2.003			−0.426	0.830	0.362
			2.007	2.007		0.245	0.490	−0.836
			2.010			−0.871	−0.267	−0.412
	P_1	A	1229		−165	−0.462	0.512	−0.724
			1234	1394	−160	0.745	0.667	−0.004
			1718		324	0.481	−0.541	−0.690
	P_2	A	183		−32	0.341	0.467	−0.816
			188	215	−27	0.809	0.297	0.508
			275		60	0.480	−0.833	−0.276

[a] A in megahertz. [b] The ESR reference x axis was chosen along the long side of the rectangular crystal; y and z were chosen mutually orthogonal and perpendicular to the faces of the crystal. The second orientation is related to (x,y,z) by $(\bar{x},y,z)$.

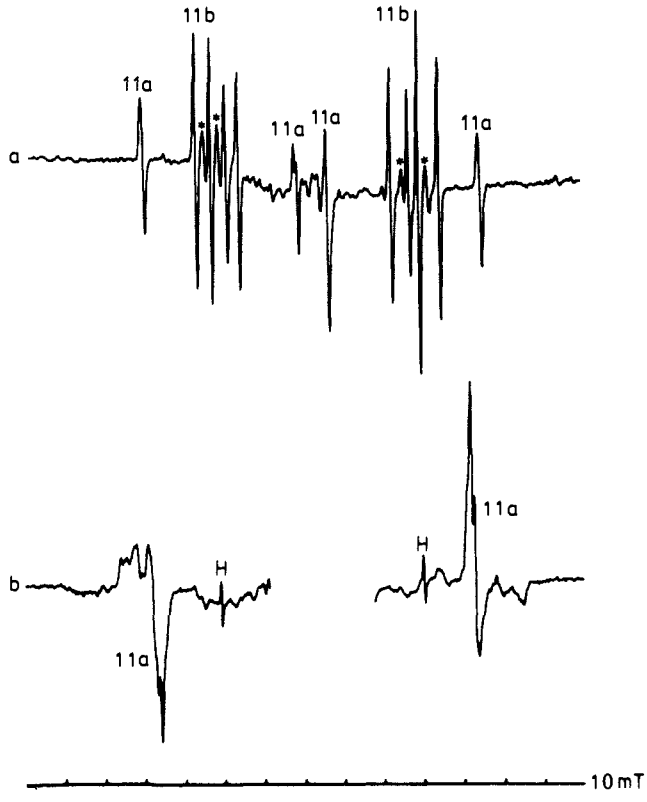

Figure 21. ESR spectra of X-irradiated 1-methyl-1,2,2-triphenyldiphosphine disulfide (**11**): (a) single-crystal spectrum at 105 K showing the transitions of radicals **11a**, **11b**, and an unidentified species, indicated with an asterisk; (b) spectrum of **11a** in a THF host matrix.

Table XIII. Relative Orientation (deg) of the Principal Directions[a] of the Hyperfine Coupling for Radicals Formed in **11**

radical	**11a**	**11b$_1$**	**11b$_2$**
11a	0		
11b$_1$	42.5	0	
11b$_2$	21.0	29.4	0

[a] Because no absolute sign can be attributed to the direction of a principal value, there is an ambiguity of ±180° in the listed angles.

creases upon annealing. This experiment discloses two important aspects relevant to radical formation in diphosphine disulfides. First, the discrimination between symmetric and asymmetric spin density distributions as observed for **1** and **2** is not the result of a small asymmetry of the precursor molecule, since the intrinsic difference of the two contiguous phosphorus moieties of **11** does not inhibit the formation of a symmetric P–P σ^* radical. Second, the dissociation reaction, which gives a confirmation of the decreased stability of the P–P bond, is not observed in the tightly packed crystalline matrix but is geometrically allowed in the randomly oriented THF environment.

1,1-Dimethyl-2,2-diphenyldiphosphine Disulfide (12). The powder spectrum of X-irradiated **12**, recorded at 105 K, reveals the presence of at least two phosphoranyl-type radicals, **12a** and **12b** (Figure 23a), and their spectral parameters are comprised in Tables III and IV.

Upon annealing, radical **12a** is readily lost at 125 K, and further warming results in the formation of a secondary radical **12c** at 215 K. Radicals **12b** and **12c** are irreversibly lost upon further warming at 235 and 250 K, respectively. Radical **12a** displays the spectral features of a symmetrical P–P σ^*-type radical, and again such a radical is formed even in a molecule in which the halves are completely different. Radical **12b** shows the intense absorption pattern of a radical exhibiting hyperfine interaction

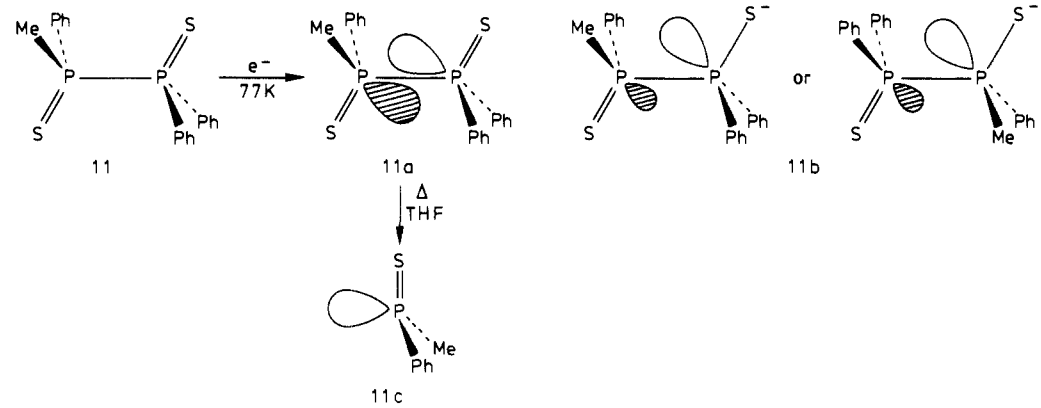

Figure 22. Structure of radicals **11a** and **11b** formed upon X irradiation of **11**.

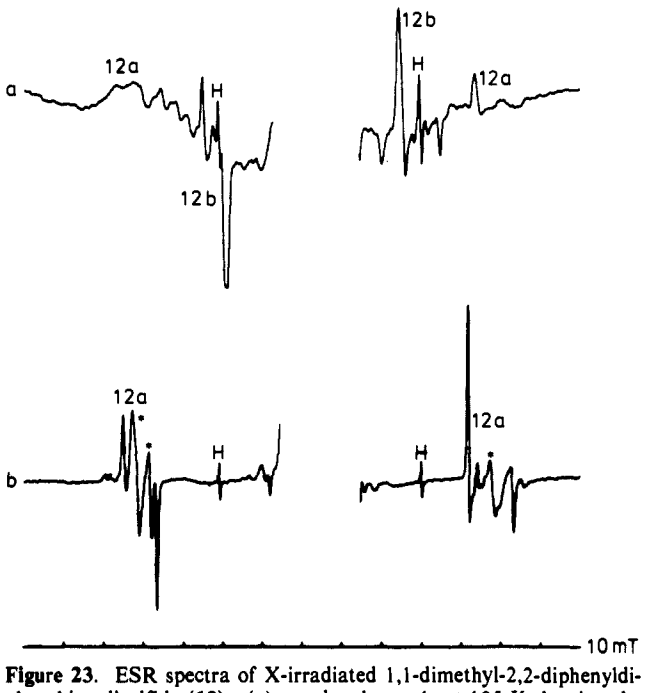

Figure 23. ESR spectra of X-irradiated 1,1-dimethyl-2,2-diphenyldiphosphine disulfide (**12**): (a) powdered sample at 105 K showing the transitions of radicals **12a** and **12b**; (b) **12a** and a related radical, indicated with an asterisk, in a THF host matrix at 105 K.

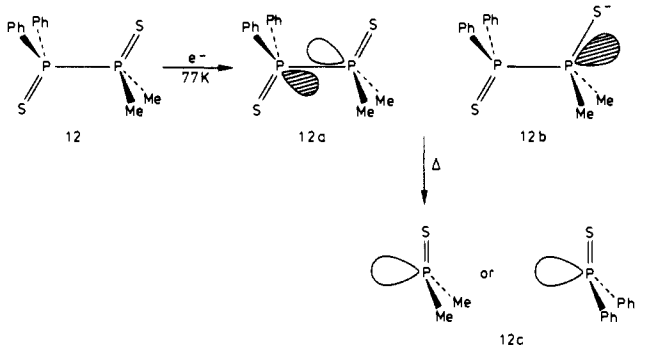

Figure 24. Structure of radicals **12a–12c** formed upon X irradiation of **12** and subsequent annealing.

with only one phosphorus atom, and we assign it to an asymmetrical P∴S σ^*-type radical. Radical **12c** reveals hyperfine interaction with a single ^{31}P nucleus and, on the basis of the spin Hamiltonian parameters, is attributed to a dissociation product, resulting from a rupture of the phosphorus–phosphorus bond (Figure 24).

X irradiation of **12** at 77 K, in frozen THF, results in the ESR spectrum given in Figure 23b. The spectrum shows clearly the outmost lines of the P∴P σ^* radical (**12a**) and is further characterized by the absence of P∴S σ^* (**12b**) or TBP-*e* configurations. The low- and high-field manifolds of **12a** possess a rather complicated appearance, and the broad transitions indicated with an asterisk (Figure 23b) might originate from an alternative P∴P σ^* configuration, somewhat different from the sharp transitions assigned to **12a**.

Discussion

The present results demonstrate that stereochemical and environmental effects can be decisive for the formation of phosphorus-centered radicals in diphosphine disulfides derivatives. The most striking result is that X irradiation of the crystalline meso compounds **1** (MePhP(S)P(S)MePh), **7** (Me(*p*-Tol)P(S)P(S)Me(*p*-Tol)), and **9** (Ph(PhCH$_2$)P(S)P(S)Ph(CH$_2$Ph)) does not lead to the usual P∴P σ^* configuration but invariably results in the formation of alternative radical configurations in which the unpaired electron is primarily located on half of the molecule, i.e., a spin-localized structure. X irradiation of the corresponding crystalline racemic forms (**2**, **8**, **10**), on the other hand, gives rise to the symmetrical P∴P σ^* configuration (spin-delocalized). It appears that the observed discrimination between symmetric (spin-delocalized) and asymmetric (spin-localized) configurations is an unique property of substituted diphosphine disulfides with aromatic substituents directly linked to the phosphorus nuclei. The marked difference in radical formation of meso and racemic diastereoisomers is not observed for diphosphine disulfides with four aliphatic substituents and seems not to be related to the size or bulkiness of the ligands. Accordingly, X irradiation of *rac*-MeEtP(S)P(S)MeEt (**4**) results in P∴P σ^* radicals, and the meso form (**3**) gives both symmetric and asymmetric species. Likewise for *meso*- and *rac*-Me(*t*-Bu)P(S)P(S)Me(*t*-Bu) (**5** and **6**) only small differences are encountered between radical formation in the diastereoisomers. In part this close agreement was not to be expected in advance, because the molecular conformation of the racemic molecules (**6**) is characterized by a gauche conformation of the sulfur atoms, completely different from the usual trans location of other diphosphine disulfides. Especially the formation of a symmetric P∴P σ^* radical is therefore to be noted.

Besides the nature of the substituents, we investigated the possibility that a small geometry distortion of half of a symmetric diphosphine disulfide precursor directs the unpaired electron to one of the two phosphorus nuclei. Such a distortion is mimicked by the precursors MePhP(S)P(S)Ph$_2$ (**11**) and Me$_2$P(S)P(S)Ph$_2$ (**12**), which incorporate an intrinsic asymmetry between the two phosphorus moieties. Nevertheless, X irradiation of the crystalline compounds generates, among spin-localized structures, unmistakable radical configurations with equal spin density on the two phosphorus nuclei. Hence, it can be concluded that the formation of a P∴P σ^* radical is not likely to be inhibited by small symmetry distortions.

The excellent agreement between the results of the X-irradiated meso compounds containing aromatic substituents directly linked to the two phosphorus atoms indicates that there exists a mutual driving force that precludes the formation of symmetric P∴P σ^* radicals. Explanation for this phenomenon cannot be purely based on intrinsic molecular properties of the isolated molecules. This is evident from the experiments in a frozen THF host matrix. X irradiation of the meso form of Ph(PhCH$_2$)P(S)P(S)Ph(CH$_2$Ph) (**9**) in a THF matrix gives the P∴P σ^* radical, completely different from the P∴S σ^* radical encountered in the crystalline compound, but almost indistinguishable from the P∴P σ^* configuration of the racemic form (**10**). This experiment demonstrates that environmental effects, possibly in combination with intramolecular forces, are very important to explain radiogenic radical formation in the crystalline compounds.

It is clear that the rate of stabilization of an initial electron-capture product toward a stable configuration determines the overall radiation process. Provided geometry relaxation is fast and leads to sufficiently deep traps, the anion radicals can be detected via ESR spectroscopy.[38] This concept gives an opportunity to explain the strong differences between the radiogenic formation of P∴P σ^* configurations in the aromatic substituted meso compounds (**1**, **7**, **9**) and the racemic analogues (**2**, **8**, **10**). Upon formation of a P∴P σ^* radical, the P–P bond will acquire some antibonding character and tend to elongate. This relaxation must be accommodated by the crystal lattice and will be strongly influenced by neighboring molecules. Fortunately, it is possible to probe the environments of the crystalline compounds via X-ray crystallographic analysis and to mimic the solid-state reaction involved in the radiation process. For several of the compounds studied, X-ray crystallographic data are available: **1**,[15] **5**,[16] **6**,[16] **7**, and **8** (vide supra). In addition we performed a crystallographic analysis on *rac*-**2** (Table II). This compound crystallizes in the triclinic $P\bar{1}$ space group with one *R*,*R* and one *S*,*S* molecule in the unit cell (a = 6.873 Å, b = 9.052 Å, c = 13.698 Å, α = 94.50°, β = 91.85°, γ = 112.05°). The P–P bond distance in the molecules is 2.240 (2) Å. The SPPS torsion angle of 158.3 (1)° indicates a significant deviation from the characteristic trans

(38) Symons, M. C. R. *Pure Appl. Chem.* **1981**, *53*, 223.

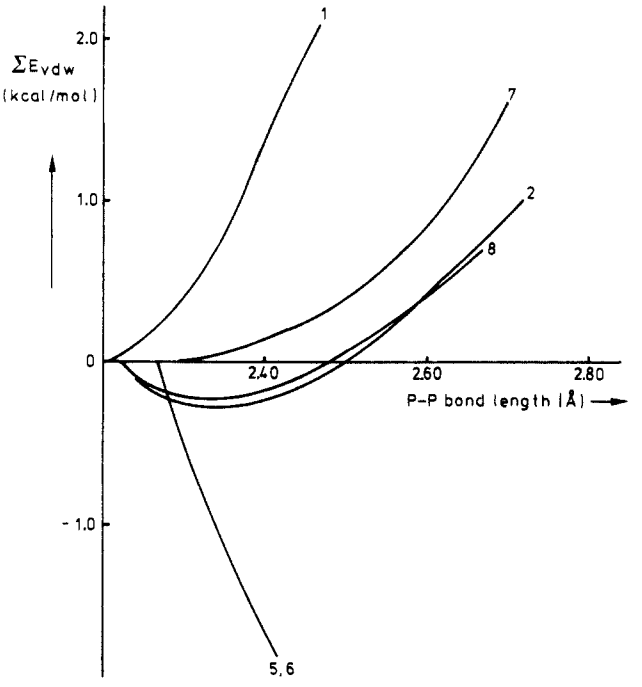

Figure 25. Change in the sum of the van der Waals energy calculated as a function of the P–P bond length in the crystal lattices of **1**, **2**, and **5–8**.

conformation generally observed in diphosphine disulfides. Despite the absence of an internal symmetry element, there are only minor differences in the bond distances and angles of the halves of the molecules, which are also in close agreement with those of related structures.[15,16,34-36] The X-ray data allow a calculation of the change in van der Waals energy as a function of the P–P bond length. The meso compounds **1**, **5**, and **7** possess a crystallographic inversion center on the P–P bond, relating the two identical phosphorus moieties of the molecule. The energy difference resulting from an elongation of the P–P bond in the meso molecules will therefore be the sum of two identical contributions. For the racemic compounds **2**, **6**, and **8**, on the other hand, there is no internal symmetry in the molecule. Hence, the two phosphorus moieties experience different steric interactions, giving unequal contributions to the total change in van der Waals energy. To overcome this problem in the calculations, we first determined the energy for elongation of each half independently and afterward constructed the curves depicted in Figure 25 by summing the separate isoenergetic bond length elongations and doubling the required energy. From Figure 25 it is evident that the meso compounds **1** and **7** suffer the most from steric interactions with their crystalline environment. This result is in complete agreement with the X-irradiation experiments giving no P∴P σ^* configurations in crystals of these compounds. For the *rac*-**2**, -**6**, and -**8**, and *meso*-**5** the change in van der Waals energy is calculated to be initially negative and apparently low enough (Figure 25) not to obstruct formation and stabilization of a P∴P σ^* radical in the crystal lattice. In the meso isomer **1** the largest contribution to the rise of the van der Waals energy comes from the interaction of the sulfur atoms with the peripheral hydrogen atoms (Figure 26a). For the racemic isomer **2**, positive contributions result from hydrogen–hydrogen interactions (Figure 26b), whereas a lowering of the steric energy comes from the release of the *intra*molecular interactions between sulfur and the methyl hydrogens on the contiguous phosphorus moiety.

It can be expected that in case stabilization of the initial electron adduct via P–P bond length elongation is unfavorable because of intermolecular restrictions, other relaxation pathways will become accessible, resulting in either an alternative phosphoranyl radical configuration (e.g., TBP-e or P∴S σ^*) or the loss of the extra electron. In this respect it can be noted that the presence of an aromatic substituent with a nearly perpendicular orientation of the aromatic ring and the P–P bond, as in **1** and

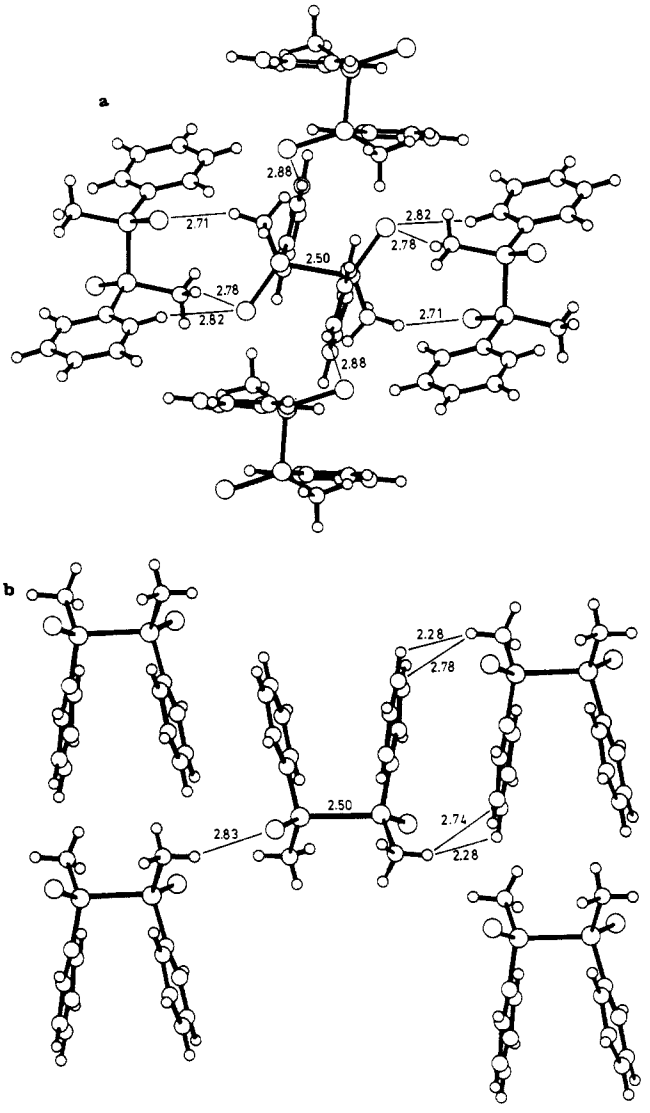

Figure 26. Crystal lattices of *meso*-**1** (a) and *rac*-**2** (b), showing the most important steric interactions resulting from an elongation of the P–P bond to 2.5 Å.

7, can be favorable for the transfer of the unpaired electron from an initial P∴P σ^* configuration to the aromatic ring because of the overlap of the aromatic π orbitals with the P∴P σ^* orbital. This provides a convenient path for the molecule either to form an aromatic anion radical or to lose the electron to the matrix, ultimately leading to recombination of the electron with the parent cationic species.

Another point that must be noted is that X irradiation of the diphosphine disulfides in a frozen THF matrix almost invariably results in a single radical product, being a P∴P σ^* configuration. Only the two *tert*-butyl-substituted compounds **5** and **6** behave differently and give spin-localized radicals as major products. The ESR spectra of **5** and **6**, however, are mutually nearly identical. The general tendency of diphosphine disulfides to give only P∴P σ^* radicals in a frozen THF host matrix can be explained by the absence of strong intermolecular interactions. It seems reasonable to assume that in a randomly oriented solid matrix the molecular packing is less tight than in a molecular crystal and that more space is available to the precursor molecules. Upon electron capture, the newly formed radical will tend to adjust its geometry via bond stretching or bond bending, which will be more favorable if the reaction cavity is larger. Hence, we propose that since steric interactions do not strongly influence the molecular relaxation in a frozen matrix, X irradiation of precursor molecules in such a host environment will result in the configuration of lowest total energy, which appears to be the P∴P σ^* structure.[39] According

to this principle, only a single radical product is formed in the frozen solutions, whereas X irradiation of crystalline samples often give rise to a number of different species.

It is interesting to note that despite the fact that the type of radicals formed upon X irradiation strongly depends on the packing of the precursors neighboring molecules, the spin density distribution of the resulting configurations is not seriously affected by the environment. This conclusion is based on the result that the valence-orbital spin densities of the respective configurations lie within a close range for the different compounds. Inspection of Table III reveals that the phosphorus valence s contribution, ρ_s, for all P∴P σ^* radicals in the crystalline solid state lies between 9 and 11% and the corresponding ρ_p value between 21 and 30%. Likewise, narrow intervals are found for the TBP-*e* configurations (ρ_s = 11.5-12.5%, ρ_p = 24-27%), the P∴S σ^* radicals (ρ_s = 12-14%, ρ_p = 37-54%), and the dissociation products (ρ_s = 6-8%, ρ_p = 41-57%). For the P∴P σ^* radicals it is also possible to compare the results from the crystalline state and the THF matrix. It appears that in THF ρ_s has decreased by approximately 0.5% and that the ρ_p values lie in a somewhat larger interval (19-28%).[30] The results demonstrate that the spin density distribution of a specific configuration is fairly constant over the various diphosphine disulfide derivatives and only slightly influenced by its environment. A similar conclusion was obtained in experiments on P∴Cl σ^* radicals.[5]

We conclude that a factor of considerable importance in the radiogenic formation of radicals in molecular crystals is the fact that the reaction cavity can constrain the movements of the precursor and modulate the necessary geometry relaxation that accompanies the formation of a stable radical product. It has been shown that *if the restraint of the environment inhibits the formation of the radical configuration energetically preferred by the isolated molecule, secondary relaxation modes become accessible leading to alternative structures.* This provides a unique possibility to study molecular states that are usually undetected. In agreement with this principle, recent experiments reveal that organic photoreactions in the crystalline state tend to occur with a minimum of deformation of the three-dimensional crystal lattice, being topochemically controlled.[10-14,37] This leads to the conclusion that the intrinsic reactivity of a molecule can be less important than the nature of the packing of its neighboring molecules.

The most illustrative example of this concept is given by our experiments on *meso*-1,2-dibenzyl-1,2-diphenyldiphosphine disulfide (**10**). In its crystalline environment, X irradiation results in the exclusive formation of an electron-capture product in which the extra electron is confined to one of the two contiguous phosphorus moieties (spin-localized). In contrast, X irradiation of the same compound in a frozen THF host matrix gives selectively the spin-delocalized three-electron bond P∴P σ^* radical.

It will be of interest to determine structure-reactivity relationships for radical precursors in the solid state on the basis of a detailed knowledge of their microenvironment.

Acknowledgment. This investigation has been supported by The Netherlands Foundation for Chemical Research (SON) with financial aid from The Netherlands Organization for Scientific Research (NWO).

Supplementary Material Available: ESR spectra of several THF-matrix experiments, angular dependence of ESR field transitions for radicals generated in compounds **5**, **7**, **8**, and **11**, and tables of fractional coordinates, thermal parameters, and molecular geometries of **2**, **7**, and **8** (16 pages); tables of observed and calculated structure factors of **2**, **7**, and **8** (58 pages). Ordering information is given on any current masthead page.

(39) It is well-known that in protic and etheric solutions it is possible to observe specific electron-gain processes (see e.g., Symons[38]). This is the result of efficient trapping of positive holes created in the radiation process and the generation of highly reactive pretrapped electrons. In the present case there is no evidence of a specific chemical effect of the solvent on the phosphorus-centered radicals or a reaction of the solute with radicals formed from the solvent.

Ab Initio Calculations on the Structure of Pyridine in Its Lowest Triplet State

W. J. Buma,† E. J. J. Groenen,*,† and M. C. van Hemert‡

Contribution from the Center for the Study of Excited States of Molecules, Huygens Laboratory, P.O. Box 9504, and Department of Chemistry, Gorlaeus Laboratories, P.O. Box 9502, University of Leiden, 2300 RA Leiden, The Netherlands. *Received November 13, 1989*

Abstract: Recently we have experimentally shown that pyridine-d_5, as a guest in a single crystal of benzene-d_6, adopts a boatlike structure upon excitation into the lowest triplet state T_0. Here MRDCI ab initio calculations are presented that reveal that the observed nonplanarity of the molecule is not caused by the crystal field but is an intrinsic property of pyridine in T_0. The origin of the distortion may be found in the nature of the π-electron system. In the lowest triplet state it is no longer a 6π-electron system as in the ground state but, in first approximation, a 7π-electron system, in which the extra electron occupies a π^* orbital that is strongly antibonding between the nitrogen atom and the ortho carbon atoms. The lowest triplet state can not be simply interpreted as an $n\pi^*$ or a $\pi\pi^*$ state.

I. Introduction

Pyridine presents the simplest molecule among azaaromatic compounds and is considered to be the model for the study of the photochemistry and photophysics of such molecules. Consequently, its lowest excited states have amply been investigated, both theoretically and experimentally. Quantum chemical calculations have been primarily aimed at the localization of the $n\pi^*$-excited states, states that do not occur in the related hydrocarbon benzene. From an experimental point of view, progress was, despite all efforts, limited for a long time. This particularly concerned pyridine's lowest triplet state T_0, due to the virtual impossibility of detecting electronic transitions to and from this state.

In a recent series of papers[1-4] on the lowest triplet state of

† Center for the Study of Excited States of Molecules.
‡ Department of Chemistry.

(1) Bos, F. C.; Buma, W. J.; Schmidt, J. *Chem. Phys. Lett.* **1985**, *117*, 203.
(2) Buma, W. J.; Groenen, E. J. J.; Schmidt, J. *Chem. Phys. Lett.* **1986**, *127*, 198.

0002-7863/90/1512-5447$02.50/0